2016

Characterization of Performance of a 3D Printed Stirling Engine Through Analysis and Test

Julie Vodhanel

CHARACTERIZATION OF PERFORMANCE OF A 3D PRINTED STIRLING

ENGINE THROUGH ANALYSIS AND TEST

Julie K. Vodhanel

Bachelor of Science in Mechanical Engineering

Case Western Reserve University

December 2000

submitted in partial fulfillment of requirements for the degree

MASTER OF SCIENCE IN MECHANICAL ENGINEERING

at the

CLEVELAND STATE UNIVERSITY

December 2016

We hereby approve this thesis for

Julie Vodhanel

Candidate for the Master of Science in Mechanical Engineering degree for the

Department of Mechanical Engineering

and the CLEVELAND STATE UNIVERSITY

College of Graduate Studies

_____

Thesis Chairperson, Dr. Mounir Ibrahim

_____

Department & Date

_____

Thesis Committee Member, Dr. Asuquo Ebiana

_____

Department & Date

_____

Thesis Committee Member, Dr. Majid Rashidi

_____

Department & Date

Student's Date of Defense: December 7, 2016

CHARACTERIZATION OF PERFORMANCE OF A 3D PRINTED STIRLING

ENGINE THROUGH ANALYSIS AND TEST

JULIE K. VODHANEL

ABSTRACT

This thesis involves the fusion of two technologies, Stirling engines and additive manufacturing. The project began by building a Stirling engine primarily out of 3D printed parts. Methods to measure the power output were designed and built with a combination of 3D printed and off the shelf parts. The Stirling engine was tested to see if there was a correlation to analysis results, and a regenerator was installed to determine the effect on performance for this relatively low temperature engine. Finally, variations in test operation and the use of heat sinks were used to find a combination that will allow the unit to run more reliably.

One challenge of the 3D printed parts was the durability when subjected to heat and assembly loads, especially over multiple rebuilds. However, the convenience of 3D printing made it possible to print replacement parts easily. New designs and assemblies were also created as a part of the effort to develop a power measurement system.

Power output was measured and corresponded to analysis predictions. Testing was conducted with a hot plate temperature of 349K (168 F) and a cold plate temperature of 308K (94 F), which corresponds to a Temperature Ratio of 1.13. Rate of rotation was 150 RPM, or 2.5 Hz. The net power output was measured to be 3.1mW. Adding that to the

losses attributed to engine friction resulted in a gross power output of 17mW, which was close to the analysis prediction of 15mW. Regenerator testing showed that using a regenerator, on average, doubled the speed of rotation at the same temperature ratio. However, the regenerator was detrimental to long term operation because without active cooling, the cold plate was unable to dissipate the heat efficiently enough. Increasing the cold side heat transfer to ambient would be essential in increasing reliability. The addition of heatsinks to the cold side was tested to determine the effectiveness, with positive results. The heatsinks that were used in testing were also analyzed, and it was determined that the spacing was too narrow for optimum performance. For future designs, custom heatsinks could be used that maximize the natural convection of the cold side, or a method developed to provide active cooling.

TABLE OF CONTENTS

LIST OF TABLES

LIST OF FIGURES

NOMENCLATURE

3D	Three Dimensional
A	Area
ABS	Acrylonitrile-Butadiene-Styrene
ABSplus™	Stratasys production-grade thermoplastic
AMF	Additive Manufacturing Format
B	Magnetic Flux Density
β	Coefficient of Volume Expansion, [1/K]
Be	Beale Number
C	Celsius
cm	Centimeter
C_p	Specific Heat at Constant Pressure
C_v	Specific Heat at Constant Volume
Δ	Delta (Difference)
DC	Direct Current
Deg	Degree
F	Fahrenheit
f	Frequency
FDM	Fused Deposition Modeling
g	Gravitational Acceleration
Gr	Grashoff Number
h	Height

ix

h_c	Heat Transfer Coefficient
Hz	Hertz
I	Inertia
K	Kelvin
KE	Kinetic Energy
kW	Kilowatt
L	Length
m	Mass
mA	Milliamp
mm	Millimeter
MPa	Mega Pascal
mW	Milliwatt
η	Efficiency
n	Ratio of Specific Heats
N	Number of Turns
NASA	National Aeronautics and Space Administration
p	Pressure
Pa	Pascal
Pr	Prandtl Number
Q_{in}	Power In, or Heat In
Q_{out}	Power Out, or Heat Out
Q_{net}	Net Power Out
q	Heat Transferred per Unit time

Ra_L, Ra_S	Rayleigh Number
RPM	Rotations per Minute
S	Spacing Between Adjacent Heat Sink Fins
STL	Standard Tessellation Language
t	Time
T	Temperature
T_c, T_{cold}	Cold Plate or Cold Space Temperature
T_f	Film Temperature
T_h, T_{hot}	Hot Plate or Hot Space Temperature
Tr	Temperature Ratio [K/K]
T_s	Surface Temperature
T_∞	Ambient Temperature
V	Volume
V	Volts
ν	Kinematic Viscosity of the Fluid [m^2/s]
W	Watt
W_{in}	Work In
W_{out}	Work Out
ω	Angular Velocity

CHAPTER I

INTRODUCTION & MOTIVATION

Additive Manufacturing is defined as the joining of materials to make an object, as opposed to subtracting material as part of the traditional manufacturing process (Campbell, Williams, Ivanova, & Garrett, 2011). Additive Manufacturing typically begins with a Three Dimensional (3D) model, which is processed by specialized software to break it down into cross sectional layers. A 3D printer then creates the part from the bottom up one layer at a time.

Three-dimensional printing started out primarily as a form of rapid prototyping, typically used to create a model of a building or of an automobile for visualization of a concept, or fit-check of a design. But due to the manufacturing advantages it offers, it has evolved into a means to create end-use items. The interest in 3D printing now is shared by consumers and manufacturers.

Some of the manufacturing advantages, according the Lipson's Principles of 3D printing (Lipson & Kurman, 2013) are:

1. Manufacturing complexity is free. Costs don't increase with complexity, which is usually the case in traditional manufacturing. Because a simple part costs the same as a complex part, engineers don't have to simplify designs to manage costs.
2. Zero lead time. Part can be printed right when it is needed, so there is no need to hold inventory. Also minimizes shipping costs if parts can be made right where they are needed.

These advantages are relevant in the university setting; if lead time of prototypes were shortened, a student can design and test a theory within a semester, enjoy immediate success, or fail faster in order to get it right.

Contrary to an internal combustion, the Stirling engine is an external combustion heat engine, meaning the heat source is external and could be supplied by virtually any source. The first patent of the Stirling engine was by Robert Stirling in 1816. He was a clergyman moved to action by the tragedies caused by the explosions of steam engines, and invented an engine that would operate at lower pressures (Shelton, 1994). In 1885, British Engineer and Inventor Sir William Siemens said, "No other form of air-engine offers so many advantages, but it has also its peculiar difficulties. If the latter can be overcome, it is likely to become the air-engine of the future" (Urieli & Berchowitz, 1984).

More recently, development of a reliable engine continued at Sunpower Inc. with William Beale, who was determined to save the world with the device he believed would solve two of the most fundamental needs, power and cooling, without harming the

environment (Shelton, 1994). In addition to being more efficient than internal combustion engines, the Stirling engine is indifferent to the source of the heat. This opens the door to wider possibilities of heat sources including solar heat or the burning of biomass. Since it can operate without Chlorofluorocarbons or fossil fuels, it has the potential to end the Greenhouse Effect, ozone depletion, and our dependence on oil (Shelton, 1994).

In their 2016 annual letter, philanthropists Bill & Melinda Gates write that poverty is more than a lack of money, but a lack of the resources needed to realize their potential. Two of the main and often overlooked obstacles of the poor are the critical resources time and energy. "But if the world can put more of both into the hands of the poorest", the letter reads, "We believe it will allow millions of dreams to take flight" (Gates & Gates , 2016).

The Gates' go on to say that if we really want to help the world's poorest families, we need to find a way to get them access to energy they can afford. However, since a majority of the poor are dependent on farming and more vulnerable to climate impacts, it's imperative to do it in a way that doesn't make climate change worse.

In order to produce cheaper, cleaner energy, we must make better use of existing technologies. In their letter, the Gates were addressing high school students because they believe they will be the ones who will ultimately be solving these problems. As an institution of higher learning, Cleveland State University has a similar audience, and the ability to provide the tools needed to work on this solution.

CHAPTER II

LITERATURE REVIEW

A. ADDITIVE MANUFACTURING

Additive manufacturing is considered a disruptive technology for its potential to influence change and drive policy updates in a wide range of topics including economics, environmental issues, and security (Campbell T. A., 2013). Because of the shift in how and where parts can be manufactured, new jobs and new markets are being created, but others become obsolete.

For example, some assembly may no longer be required. 3D printing can form interlocked parts, unlike standard manufacturing, where parts are created and assembled separately. This reduces overall manufacturing time and cost. In addition, zero skill is required for manufacturing. Most of the necessary information is contained in the design file, and diminishes need for skilled production. The printers also provide precision and reliability for virtually any design, creating mass production of features previously only

available through artisan production (Lipson & Kurman, 2013). This creates the potential for additive manufacturing to eliminate jobs in assembly and manufacturing, but create more jobs for engineers, designers, and individuals with Computer aided drafting skills (Campbell T. A., 2013).

In project management, there is a concept referred to as the Iron Triangle, with the three sides being Better, Faster and Cheaper. (Swisher, 2014) The goal is to meet all three, but more often than not, a project manager is forced to pick two. The benefits of additive manufacturing can be evaluated on these criteria as well. Better is subjective, but there are measurable qualities of 3D printing that make it faster and cheaper.

Additive manufacturing can definitely be faster, as parts can be printed in a matter of hours. This is an important aspect in schools where students may only have weeks to complete a project. It's a major factor in manufacturing too, as companies are competing to be the first to market and get parts to consumers quickly.

Since overhead costs associated with tooling are eliminated, additive manufacturing can also be cheaper. If a part doesn't work the first time, the upfront investment isn't lost, only the cost of that material. It also affords engineers the ability to test fit and function of a new design before turning over to manufacturing. For example, automobile manufacturers create full scale models of concepts to evaluate ergonomics and serviceability before the prototype is cast, and have replaced or supplemented foam and clay carvings with 3D printed parts (Lipson & Kurman, 2013).

Beyond just creating prototypes for mass manufactured items, users can make custom use parts which are not subject to economies of scale. It is becoming affordable to have a 3D printer in a home, not just a factory. Do It Yourself (DIY) Innovation, also referred to as the maker movement, has become popular. One of the reasons it is successful is because it can offer an experience, not just a product (Lipson & Kurman, 2013). The process can foster a transformation, not unlike the aspiration of a traditional college education; a person gains a sense of community, the opportunity to acquire a new skill, and satisfaction of designing and manufacturing something of use.

There is also the ability to recycle and reuse. When a part becomes obsolete, as long as the material is reusable, it can be melted down and rebuilt as another part. Examples include toys, cell phone cases, medical casts and braces, and tools needed on the space station.

Cleveland State University decided to take advantage of these benefits and purchased five 3D printers which were installed in a dedicated laboratory on April 23, 2015. The installation included one Fortus 250mc 3D printer, four uPrint SE Plus 3D printers, and 2 solvent stations. Students were trained on two different preparation software packages, and on using the machines.

The first step in getting a part manufactured is preparing the design file. While Engineers will typically use high end software such as Pro-Engineer or Solidworks, any

software package such as Google Sketchup that exports to a language that can be read by the printer is acceptable. In other applications, such as in the medical industry, instead of creating a drawing, a scan can be done to create the model (Lipson & Kurman, 2013).

STL (Standard Tessellation Language) is the current language standard in 3D printers. According to Lipson & Kurman (2013), STL was designed to simplify model for printing, but has become a limiting factor. AMF, or Additive Manufacturing Format, uses curved triangles instead of planar. It maintains the surface mesh of STL, but AMF files have added capabilities to store information such as different colors, multiple materials, lattices and internal structures. AMF was approved as a standard in 2010 but not yet adopted by 3D print vendors (Lipson & Kurman, 2013).

The software packages installed at Cleveland State University were CatalystEX and Insight. The programs utilize different methods for determining the layers and support material needed to create the model, and transform to the .STL file. The printers then use Fused Deposition Modeling (FDM) to build the parts layer-by-layer with ABSplus™ thermoplastic (Stratasys ABSplus, 2016), and a support material. After the parts are printed, they are placed in the solvent where the support material is dissolved away, leaving only the finished part.

B. STIRLING ENGINES

Stirling engines operate on the Stirling cycle to either generate electricity or act as a heat pump. Since the factors that drive capability for a Stirling engine are external heat available and efficiency, Stirling engines are prime candidates for converting solar thermal energy to electrical. Known capability of existing engines ranges from 5W to 500W to 5kW (Ibrahim & Tew, 2012).

Stirling engines have a hot side chamber and a cold side chamber, and utilize two types of pistons, Displacer Pistons and Power Pistons. The hot side is actively heated, and the cold side actively cooled. The displacer piston moves the working fluid between the hot chamber and the cold chamber, and the power piston is the means to extract the work from the engine.

In addition to energy conversion, Stirling engines can be used as heat pumps, also known as a coolers. Opposite of an engine, a cooler needs electricity supplied to drive the piston and displacer. The pressurization and depressurization cause energy to be absorbed at one end and rejected at the other. A Stirling Cooler is typically used for food storage or electronics cooling (Ibrahim & Tew, 2012). A Stirling Cryo-cooler, which can cool below 100K, would be used for infrared sensor cooling applications (Ibrahim & Tew, 2012).

There are four general types of Stirling converters: Alpha, Beta, Gamma, and Double-acting. The Alpha has two power pistons in separate cylinders with the working

8

fluid in between. The Beta has the displacer and power piston in the same cylinder, while a Gamma has the displacer and power piston in separate cylinders, or cylinders with different diameters. A double-acting is a compound Alpha type (Martini, 1983).

In order to extract power from most engines, pistons and displacers are connected by linkages and crankshafts and have prescribed motions. These are also called Kinematic Engines. Kinematic engines typically require lubricant, mechanical seals, and bearings which can limit engine performance and life (Ibrahim & Tew, 2012). For increased reliability, William Beale and Sunpower invented a hermetically sealed version, called a free-piston engine, eliminating the external crank mechanisms (Shelton, 1994). Also called linear alternator designs, reciprocating motion of the piston, rather than rotational motion, creates the current. (Ibrahim & Tew, 2012)

For all types of converters, of critical importance to the performance of the cycle is the regenerator. The regenerator is a component that extracts thermal energy from the working fluid when it flows from hot to cold, and returns the heat to the working fluid when it moves back to the hot portion. The regenerator is critical component to target from improvement (Ibrahim & Tew, 2012), especially for coolers.

According to *Stirling Converter Regenerators* (Ibrahim & Tew, 2012), regenerators are typically made of either a stack of woven screens, random fibers, or wrapped foil. Woven screens are often expensive and difficult to manufacture, while random fibers are typically easier to manufacture and lower cost than screens. The performance of random

9

fibers is about the same as woven screens, and they both outperform the wrapped foil. Wrapped foil theoretically should provide the best performance, but they are difficult to fabricate and maintain proper spacing (Ibrahim & Tew, 2012).

The criteria for an effective regenerator is high heat transfer and low pressure drop. Minimizing pressure drop can be accomplished by providing a smooth surface, controlled flow acceleration (no abrupt expansions or contractions) while minimizing flow separation and maintaining uniform distribution throughout (Ibrahim & Tew, 2012).

An idea at the start of this project was to use the 3D printer to create a new regenerator for the NASA/Sunpower Oscillating-Flow Test Rig that is being tested in the laboratory at Cleveland State University. The regenerator currently used in this engine is expensive and has a long lead time. In addition to potentially reducing time and cost, the ability to fabricate a regenerator in 3D opens possibilities for designs that are not constrained by standard manufacturing limits, such as variable diameter or variable porosity. The design possibilities are limited only by the ability to create the model and the capability of the printer.

Initially, it was desired to print Microchannel regenerator disks (Ibrahim & Tew, 2012). Even if they weren't of an ideal thermal material, the printed parts would be useful for pressure drop and flow testing. Regenerator thermal inefficiency contributes 1.5% to thermal inefficiency while pressure drop losses contribute about 11% engine inefficiency (Ibrahim & Tew, 2012). However, the thickness resolution possible on the available 3D

printers didn't make printing the regenerator disks an option. Comparisons of the

Microchannel specifications and the printer capabilities are shown in Table I.

Table I. Regenerator Disks

Regenerator Disk Dimensions	Stratasys Fortus 250mc 3D printer Capability
OD = 19.05 mm	Three layer thickness resolutions: 0.178, 0.254 and .330mm
Involute Channel Width = 86 microns = 0.086mm	
Wall thickness between involutes: ~ 14 microns = 0.014 mm	
Wall thickness between rings : 20 microns =0.020mm	Part Accuracy: +/-0.241mm
Disk thickness: 500 microns 0.5mm	

Instead of the regenerator, it was decided to build a complete Stirling engine

primarily with 3D printed parts. The engine would be subjected to analysis and test, with

the objective to correlate performance data with analysis results, and determine the effect

of a regenerator in this particular engine.

C. STIRLING ENGINE ANALYSIS

There are various analysis methods available to estimate Stirling engine performance. The methods are classified by order, first-order, second-order or third-order, depending on complexity.

First-order design methods are the simplest method to determine power output and efficiency. In their review of Stirling Engine Mathematical Models, Chen and Griffin described them as a quick way to estimate the relationship between the overall size of an engine and its power output, but not useful as a detailed design tool (Chen & Griffin, 1983). Power output and efficiency can be estimated with three know engine parameters:

- Heater and Cooler Temperature
- Engine displacement
- Speed

First, power out is determined based on an ideal, or loss-free analysis such as the Beale number or Schmidt cycle. Then corrections for various losses and correlation factors that have been determined by experience with actual engines are used to formulate realistic output from ideal output.

The Beale Equation (Martini, 1983) is an example of a first-order design method for power estimation. According to William Beale of Sunpower Inc., the power of many Stirling engines conforms to the simple equation:

$Q_{out} = Be * p * f * V$

where

Q_{out} = Engine Power (W)

p = mean cycle pressure (MPa)

f = cycle frequency of engine speed (Hz)

V = displacement of power piston (cm^3)

Q_{out}/pfV is a dimensionless group known as the Beale number (Be), typically between 0.011 and 0.015 for the units shown above.

Beale found this number to be an applicable approximation for multiple Stirling engine types and sizes. The engines he typically worked with operated between a heater temperature of 650C (1202F) and a cooler temperature of 65C (149F).

According to analysis and testing conducted by Graham Walker (Martini, 1983), there is an important relationship between the Beale number and heater temperature, and his predictions are shown in Figure 1.
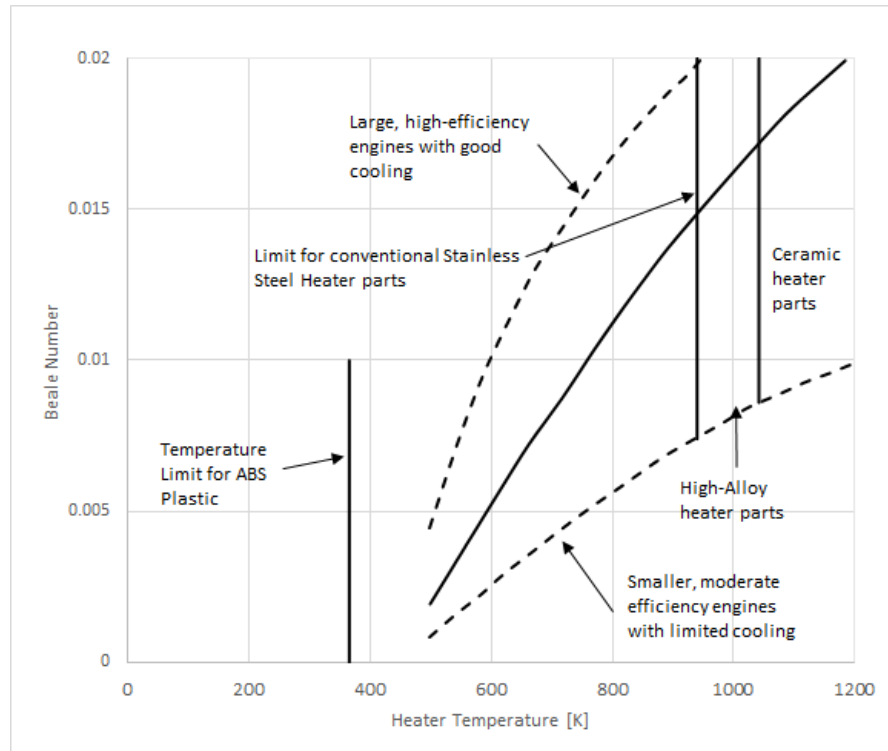
Figure 1. Beale Number as a function of Heater Temperature

Walker points out that the material operating temperature will confine the operation to a limited region. Figure 1 shows Walker's graph expanded to include the deformation temperatures of ABS plastic, which will be the upper limit for testing. It doesn't appear that Walker's prediction can be extrapolated to the relatively low heater temperatures used for the 3D printed Engine to obtain an exact value, but one order of magnitude lower, 0.0011 to 0.0015, may be reasonable, and will be used in this analysis.

The Carlqvist Formula (Martini, 1983) is an example of a first-order efficiency prediction. The Carlqvist formula starts with the Carnot efficiency and multiplies it by the

efficiencies of the heater and mechanical systems, predicting a maximum for a well optimized engine to be about 58% of Carnot.

Second-order methods are more complicated but still provide relatively simple procedures to predict performance, and to optimize a Stirling engine design. They are also referred to as a decoupled analysis, because in all second order design methods, it's assumed that energy losses are not dependent on each other. (Chen & Griffin, 1983)

To perform a second-order analysis, a simplified cycle analysis is used to determine basic power output and heat input. Power losses are subtracted from power out and heat losses are added to heat input to arrive at a net performance (Chen & Griffin, 1983). This is different from the first order methods in that individual losses are identified and quantified (Chen & Griffin, 1983).

Second-order design methods are divided into three categories, isothermal, adiabatic and semi-adiabatic. In an isothermal analysis, which is based on Schmidt isothermal cycle assumptions (Chen & Griffin, 1983), heat transfer between gas spaces and cylinder are infinite. Gas in the expanded space is equal to the heat source temperature, and gas in the compression space is equal to the heat sink temperature. Perfect regeneration is assumed.

In his Stirling Engine Design Manual, Martini described the Schmidt cycle analysis (Martini, 1983). The Schmidt cycle is a Stirling cycle in which the displacer piston and power piston move sinusoidally.

The following assumptions are made when using the Schmidt cycle equations.

- The motion of the parts is sinusoidal

- Gas temperatures in all parts of the engine are known and constant

- There is no gas leakage

- The working fluid obeys perfect gas law

- At each instant in the cycle, gas pressure is the same throughout

For an adiabatic analysis (Chen & Griffin, 1983), the compression and expansion space are perfectly insulated so that the heat transfer is equal to zero. It is more realistic than the Schmidt analysis for large engines operating at high frequencies. Gasses leave at source temperature and mix perfectly at the opposite space. Similar to an isothermal analysis, perfect regeneration is assumed.

Dr. Israel Uriel, Professor Emeritus at Ohio University, and David Berchowitz, Engineer at the former Sunpower Inc., authors of "Stirling Cycle Engine Analysis" wrote that one advantage of isothermal analysis is that equations can be explicitly integrated, and closed form solutions can be obtained with sinusoidal changes in volume. The ideal adiabatic analysis, they point out, without the isothermal assumptions, require differential equation analysis. The equations are non-linear and require numerical methods to solve.

However, the benefit would be that information on all of the variables is obtainable for each point in the cycle, making it possible to evaluate the importance of the regenerator and analyze heat exchanger components (Urieli & Berchowitz, 1984).

Also, given the same mass of working gas, adiabatic and non-isothermal performance results should not be significantly different (Urieli & Berchowitz, 1984). Thermal efficiency will be reduced from Carnot due the irreversibilities introduced in the adiabatic analysis (Urieli & Berchowitz, 1984). Power output of the adiabatic analysis is expected to be higher due to the pressure differences calculated in the polytropic processes.

pV^n = constant

Where p = pressure, V = volume

For the isothermal case, n = 1, pV = constant

For the adiabatic case, n = ratio of specific heats (C_p/C_v)

The third type of second-order analysis is the semi-adiabatic analysis, which employs a limited heat transfer rate, and lies somewhere between isothermal (infinite heat transfer rate) and adiabatic (zero heat transfer rate) (Chen & Griffin, 1983). One example is the Finkelstein method, (Chen & Griffin, 1983) which uses a limited heat transfer rate to account for heat transfer in expansion and compression spaces. Wall temperatures are constant, and equal to heat source and heat sink temperatures. The heater, cooler and regenerator are perfect. The solution requires simple numerical integration.

Third-order analysis methods, or nodal analysis, involves dividing the engine into nodes, or control volumes, and setting up differential equations for conservation of mass, momentum, and energy, and the equation of state for the working gas. Numerical methods are then used to simultaneously solve the system of differential equations. (Chen & Griffin, 1983)

CHAPTER III

PROBLEM STATEMENT

The purpose of this thesis is to build a Stirling engine primary out of 3D printed parts, and conduct a series of tests to measure performance. The three areas of focus were reliable functionality, the effect of the regenerator, and power output measurement.

The model of the Stirling engine can be an effective learning tool if it runs reliably. Losses and inefficiencies can cause the unit to deteriorate or fail. Documented in this thesis will be the issues that were encountered and methods to improve function.

In a typical Stirling engine, the regenerator is of critical importance to performance. The engines will tested with and without a regenerator to determine the effect in this relatively low temperature application.

Stirling engine performance predictions can be made based on general operating parameters. In this thesis, the specifications of the engine will be applied to analysis methods, and predictions will be compared to test data. A method to measure output power will also be designed in order to quantify performance and calculate efficiency.

CHAPTER IV

APPROACH

A. 3D PRINTED STIRLING ENGINE

Stratasys, the company who is supplying the 3D printing machines to the school, provided files for a gamma type kinematic Stirling engine. The Stirling engine appears to be a variation of an engine design created by Doug Conner and described on SolarHeatEngines.com, a website dedicated to analysis, design, and testing of solar-powered engines.

The engine parts were printed on a Stratasys Fortus 250mc 3D printer. The Stratasys uses Fused Deposition Modeling (FDM) of ABSplus plastic. The fabricated metal parts, including the hot plates, cold plates, and power piston were manufactured by David Epperly in the machine shop of the Cleveland State University model development lab.
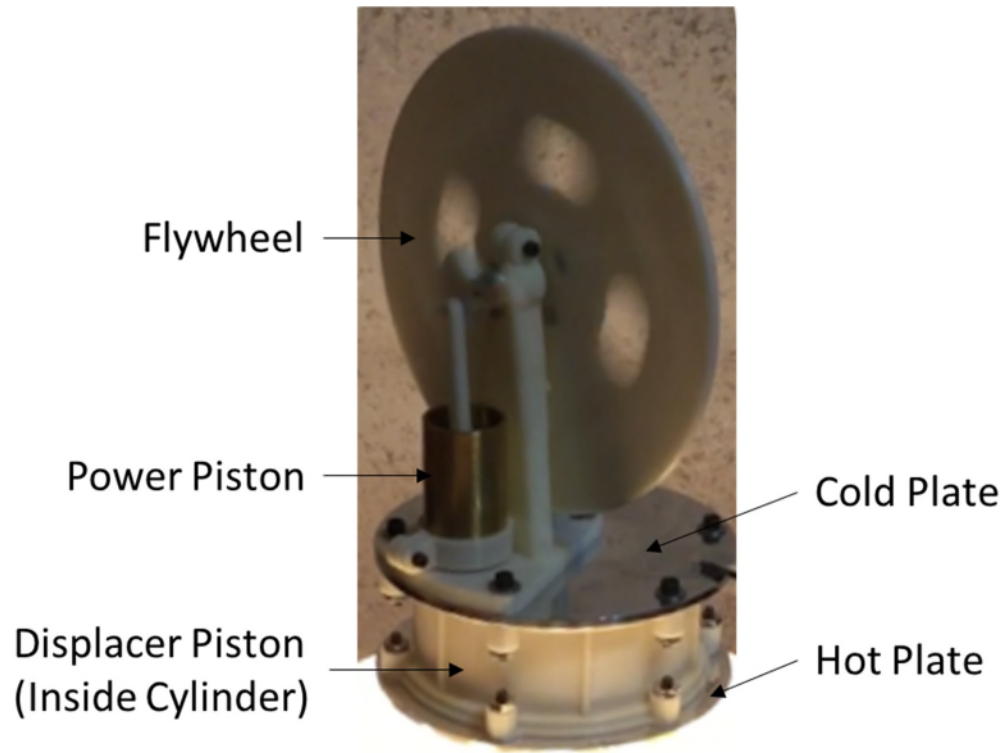
Figure 2. 3D Printed Stirling Engine

The engine is designed to run on heat from a light bulb located in a lampstand below the hot plate. The cold side is exposed to ambient for natural convective cooling. The original lampstand had the Stratasys logo, but as the first example of the modifications that are possible using the 3D printer, the design was customized.

Figure 3. Customized Lamp Base

Two engines were built, and minor variations will be described and tested in the following sections. Table II lists the features or variables that were controlled and tested.

Table II. Stirling Engine Variables

Parameter	1	2
Regenerator	Empty Cavity	Folded Fins
Flywheel	No additional weight	Weighted with magnets
Input Power	Input power is continuously variable using a sliding dimmer switch.	
Cold Side Heat Transfer	No Heatsinks	Variable number of Heatinks
	Ice used for cooling at times to control temperature ratio	

B. TEST RIG

1. Measuring Temperature, Power Input and Flywheel Rotation

      Thermocouples and digital readers were used to measure temperature during the tests. Four thermocouples were used, one for ambient temperature, one for the hot side plate, and two for the cold side plate. It was assumed that the hot plate temperature would be the same throughout, but two thermocouples were used for the cold side to make sure the temperature was also consistent.
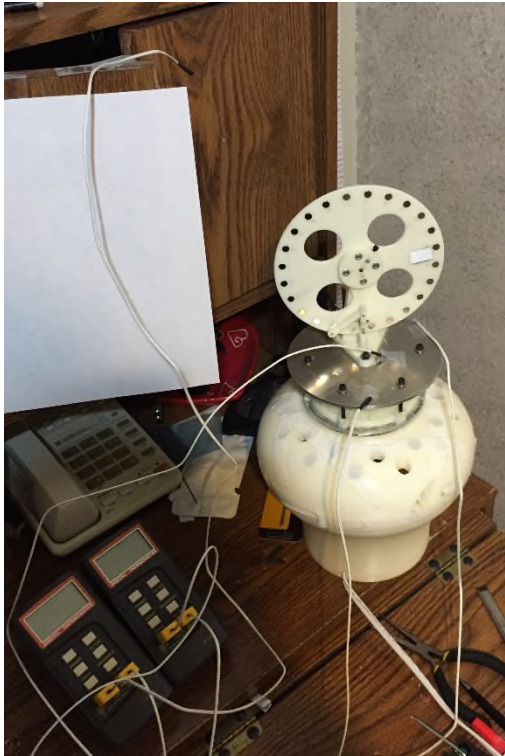

Figure 4. Thermocouple Setup

Figure 5. Thermocouple Locations

Light bulbs with different power ratings were used for testing, and when necessary, the bulb was controlled using a dimmer switch. Input power (Qin) was measured using a TS-836A Plug Power Meter.

Figure 6. Input Power Meter

The speed of rotation of the flywheel was measured using a CyberTech Digital Photo Tachometer. A reflective test strip was affixed to the wheel, and a piece of paper was posted behind the wheel to create a consistent background for measurement. Measurement units were in Rotations per minute (RPM) and converted to cycles per second (Hz) as needed.
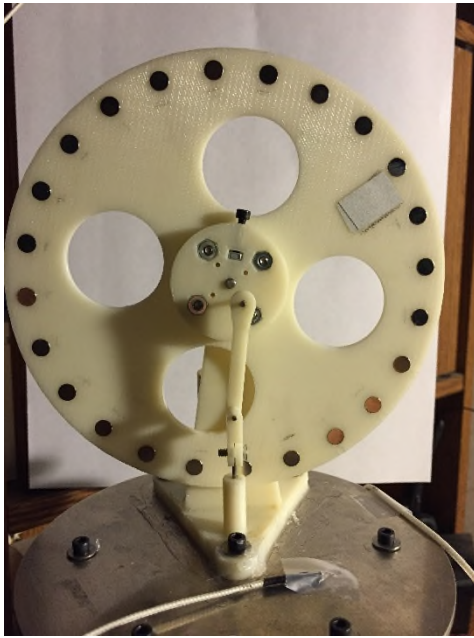

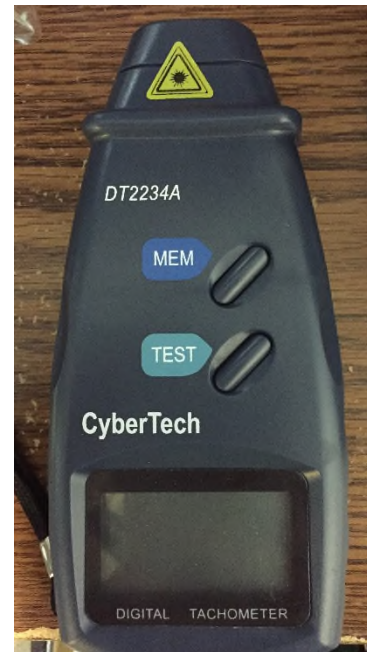
Figure 7. Flywheel with Reflective Test Strip

Figure 8. Photo Tachometer

2. Electromagnetic Power Output

A goal this thesis was to develop a method to measure power output, and compare it to analysis predictions. The first attempt at measuring output was to build a single-sided axial flux machine.

An axial flux machine is made of rotors carrying disk magnets that create an axial flux, and a stator that holds the phase windings (Price, Batzel, Comanescu, & Muller, 2008). A single-sided configuration consists of a single rotor and a single stator as shown in the figure below. (Egea, 2013)
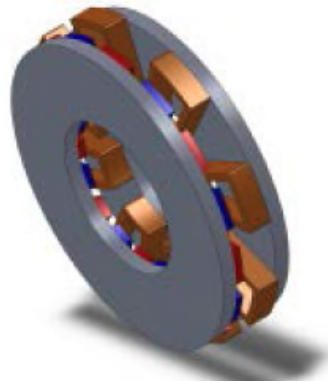

Figure 9. Single-Sided Axial Flux Machine

The Stirling engine flywheel was redesigned to accept magnets at 15 degree increments around the circumference, and the revised design was printed on the uPrint 250. Twenty-four 6mm diameter by 1.5mm thick Neodymium N35Disc Magnets were then installed into the flywheel to form the rotor. The magnets were installed in the flywheel in an alternating north and south pattern.
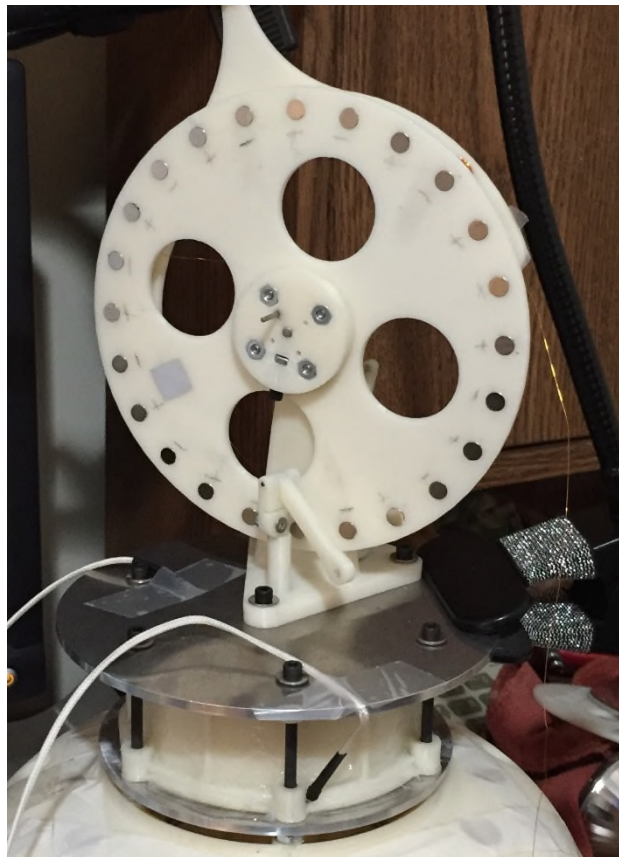

Figure 10. Flywheel with Magnets

Also designed and printed was a caliper and spools to hold the copper wire. This assembly would serve at as the stator. Thirty-six gauge copper motor winding was wound around each spool 300 times. The number of turns was determined using Faraday's law, which states that:

$$V = -N\frac{\Delta(BA)}{\Delta t}$$

Where
V = Voltage [V]
N = Number of turns
B = Magnetic Flux Density [Tesla]
A = Area of magnet [meter]
Δt = Time for 1 revolution of the flywheel

For this project, the magnets are rated to 3500 Tesla, but due to distance from the spool, 500 Tesla was used as a conservative estimate. Faraday's law was then rearranged to determine the number of turns required to provide for a rate of rotation of 100 RPM, or 0.6 seconds per revolution. Since the power of the engine is estimated to be in the 20mW range, if voltage is 7V, the current is expected to be about 3mA.
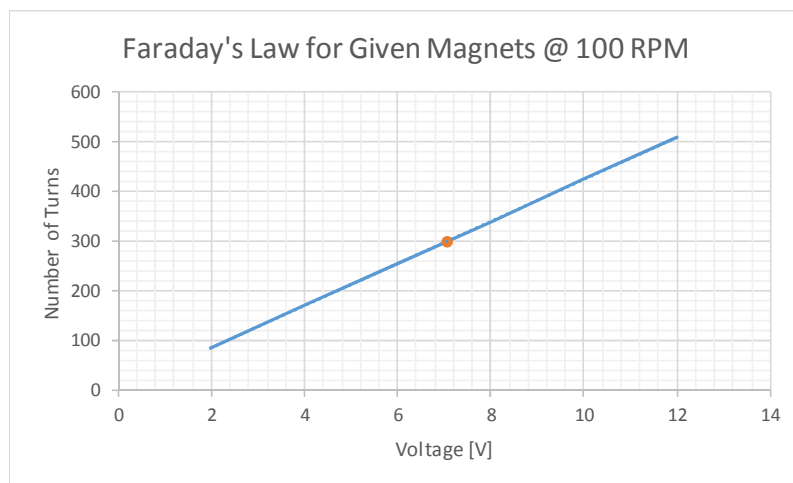

Figure 11. Results for Faraday's Law

For a single phase unit such as this, the coils are wound opposite, one clockwise and the other counterclockwise. The wire solid copper wire had a thin enamel coating to resist moisture and heat, so the enamel had to be removed with sandpaper to expose the copper at the attachment points.

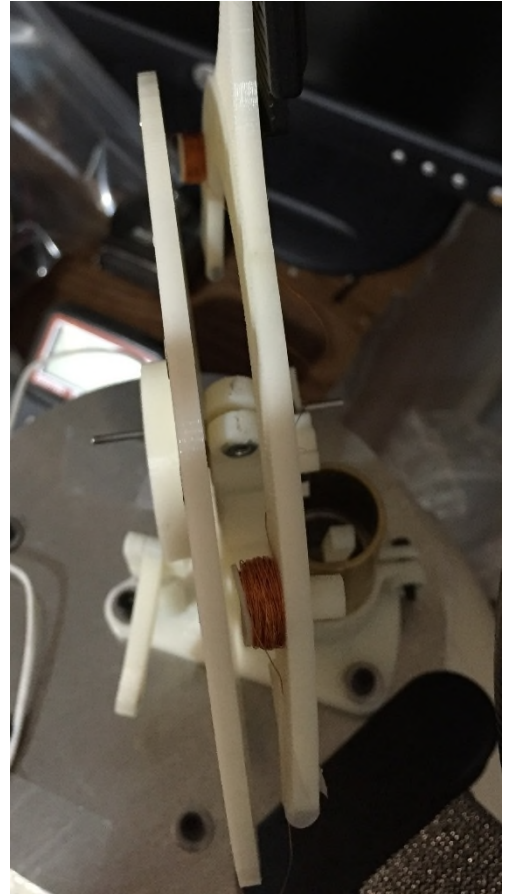

Figure 12. Stator with Wire Spools

Figure 13. Rotor and Stator

The circuit was set up according to Figure 14 to mimic a Direct Current motor configuration (Modeling DC Motor Position, 2014).
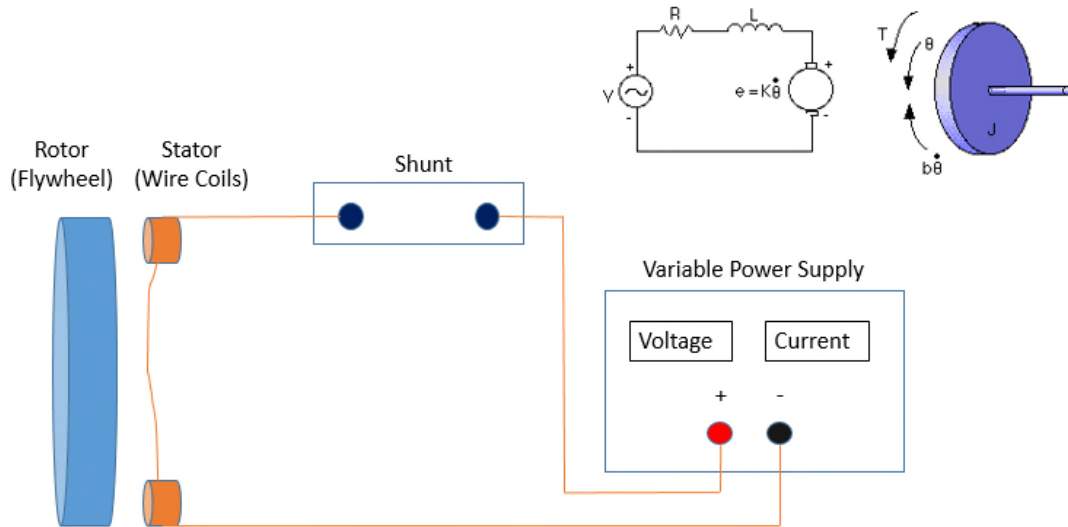

Figure 14. Braking Apparatus Circuit Diagram

3. Lifting a Weight Against Gravity

A second method to measure power output of the engine was also used in this thesis. It involved attaching a spool to one of the linkages on the engine that would wind a string that was attached to a weight. The idea is to measure the rate of change of potential energy based on the following equation:

$$Power = \frac{mgh}{\Delta t}$$

Where   m = mass of the weight

g = gravitational constant

h = height, or distance weight moves

Δt = time that the weight takes to move distance

The spool was attached in front of the linkage in a spot where it wouldn't interfere with the rotation of the flywheel past the linkage.
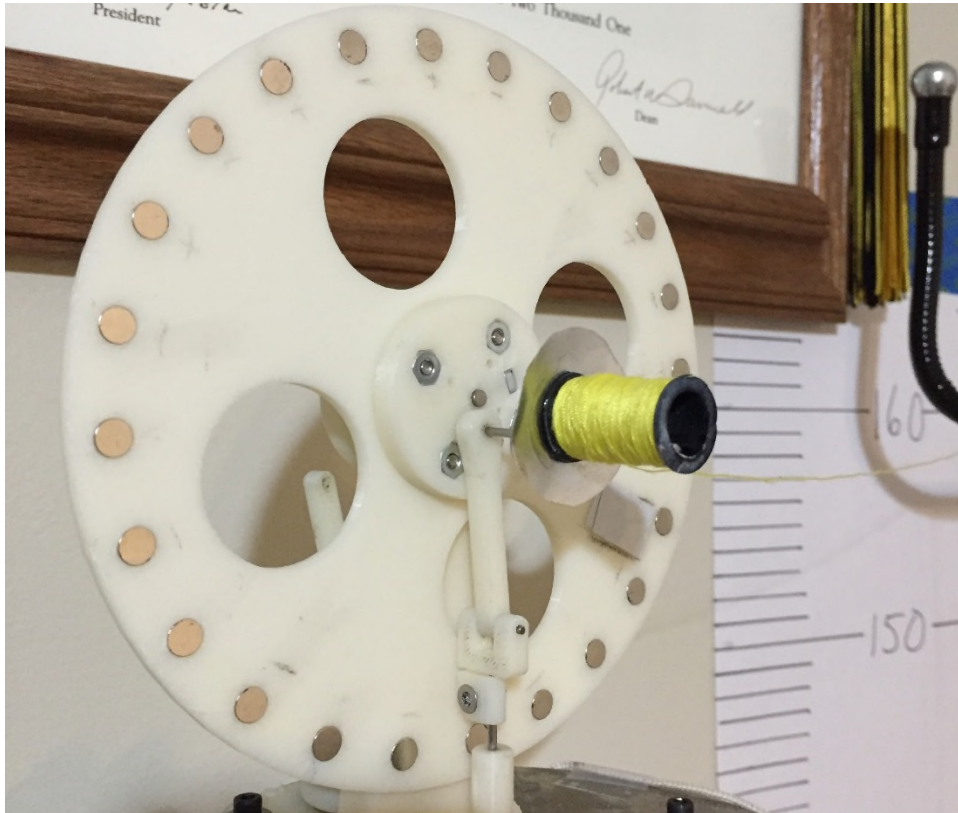

Figure 15. Spool Connection to Flywheel

The thread passed over a low friction arm. The arm was movable and positioned to guide the string over the spool. To begin the test, a few feet of slack in the thread was created between the wheel and the arm in order to make sure that when the wheel was turned by hand, the initial startup did not move the weight.
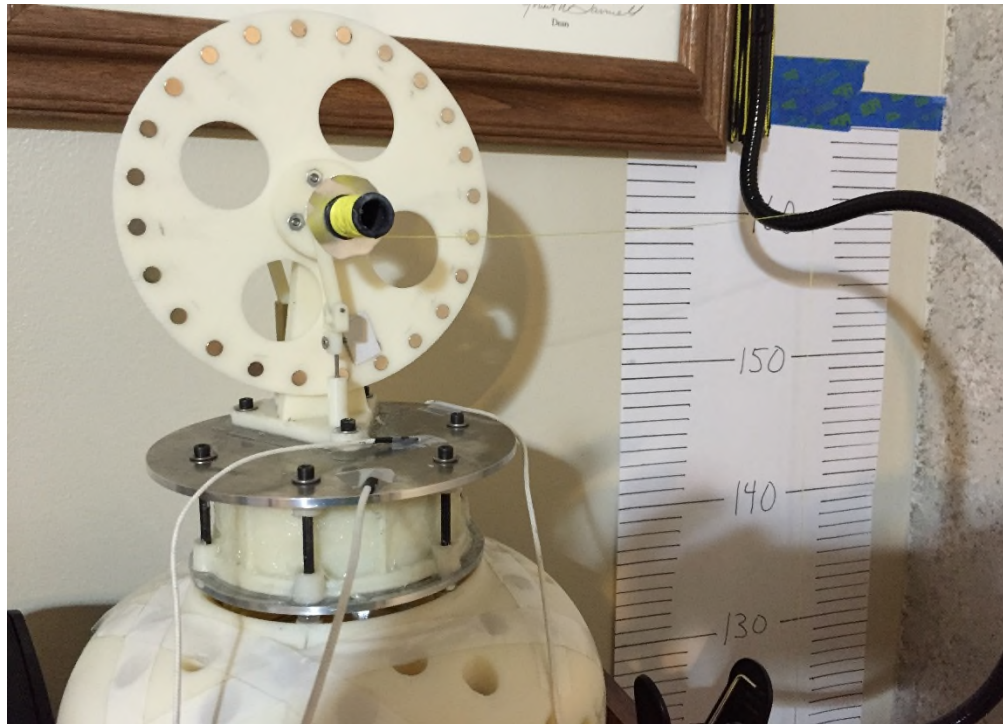

Figure 16. Spool Test Rig

A video camera was set up to record the movement of the weight during the test, and a large print metric ruler was created and posted on the wall behind the weight to show the distance covered. The results of this testing are shown in Chaper V.

Figure 17. Spool and Weight Test Setup

CHAPTER V

RESULTS AND DISCUSSION

A. STIRLING ENGINE TESTS AND RESULTS

1. Input Power

The testing variations were conducted in order to try to measure performance changes, but the testing also provided some insight into nominal operation and reliability. In all tests, 35W appeared to be the minimum input required to provide enough of a temperature rise over ambient without actively cooling the cold plate. Operation at 42W or higher is not recommended since the steady-state temperature of the plate can climb higher than the allowable temperature for the plastic parts. Power input of 40W appears to be the highest bulb rating for long term operation.

Figure 18 shows the transient temperature of the hot side plate at different power inputs. If more than 40W, over time the temperature will drift above 200°F causing the plastic to warp.
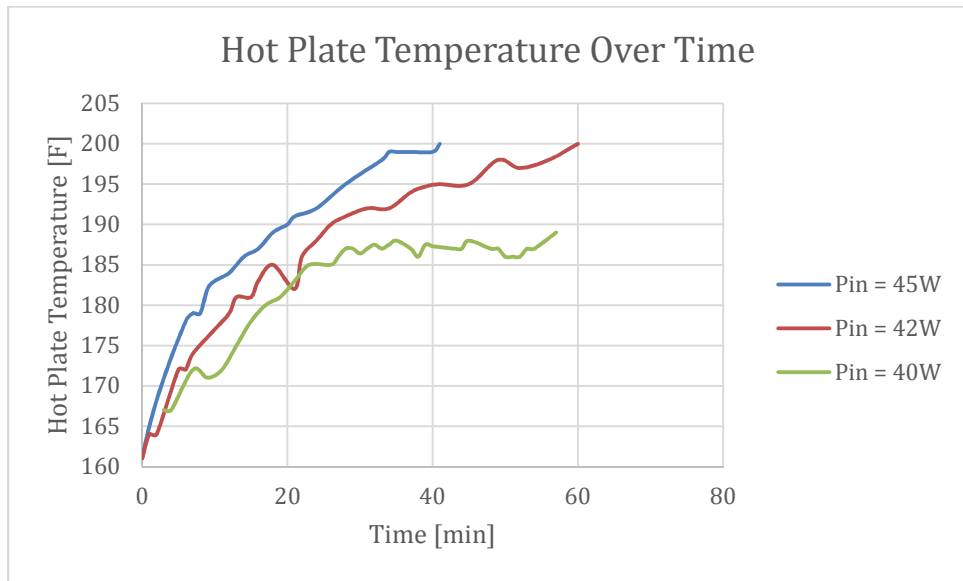

Figure 18. Hot Plate Temperature over Time at different Power Inputs

2. Cold Side Heat Dissipation

Because of the temperature limitations of the material, increasing the cold side heat transfer to ambient would be the one of the most effective factors to increasing reliability. In order to determine factors that may affect this heat transfer, additional testing was conducted with the following conditions and variables.

The tests were conducted using a 39W light bulb for the input power. The unit did not have a regenerator and the flywheel was unweighted. One thermocouple was used to monitor the hot plate, and two thermocouples were mounted on the cold plate. A fourth thermocouple monitored the ambient temperature in the room.

The variables that were tested were:

1. Proximity to the wall.

    6" from the wall, as measured from the wall to lamp base, is

    designated as "Near", and 18" will be called "Away".

2. Utilization of Heatsinks on the cold plate.

    25mm Length x 16mm Width x 16mm Height heat sinks were

    attached to the cold plate. Artic Silver thermal grease was used in

    order to reduce the thermal resistance between the plate and the

    heatsink.

The purpose of the heatsinks would be to increase the area available for natural convection. The equation for heat transfer is:

$$q = h_c \, A \, (T_s - T_\infty)$$

where q = heat transferred per unit time

A = heat transfer area of the surface

h_c = convective heat transfer coefficient

T_s = Cold plate surface temperature

T_∞ = Ambient temperature

Each heatsink, with fins 1 inch long and 0.5 inches high, and four fins per, provides almost 4 square inches of surface area per heatsink. When added to the cold plate, which is about 21 square inches total, minus areas that are covered by the 3D printed Stirling engine bracket, three heatsinks increase the surface area by 50%.

The first set of results compares the Temperature Ratio for units tested near the wall. Temperature Ratio is the ratio between the hot and cold plate temperature (T_h/T_c) and is in an absolute temperature scale (Kelvin). The unit was tested without heatsinks, then again with 3 heatsinks on the cold plate. Results are sorted by ambient temperature, which was recorded about 1.5 feet from the unit. Tests were conducted on different days, with slightly different ambient temperatures. Even with the ambient temperature difference, it appears that near the wall, with three heatsinks added the temperature ratios were higher than without. However, both tests did end in stoppage of the unit, both within 2 hours of reaching steady state.
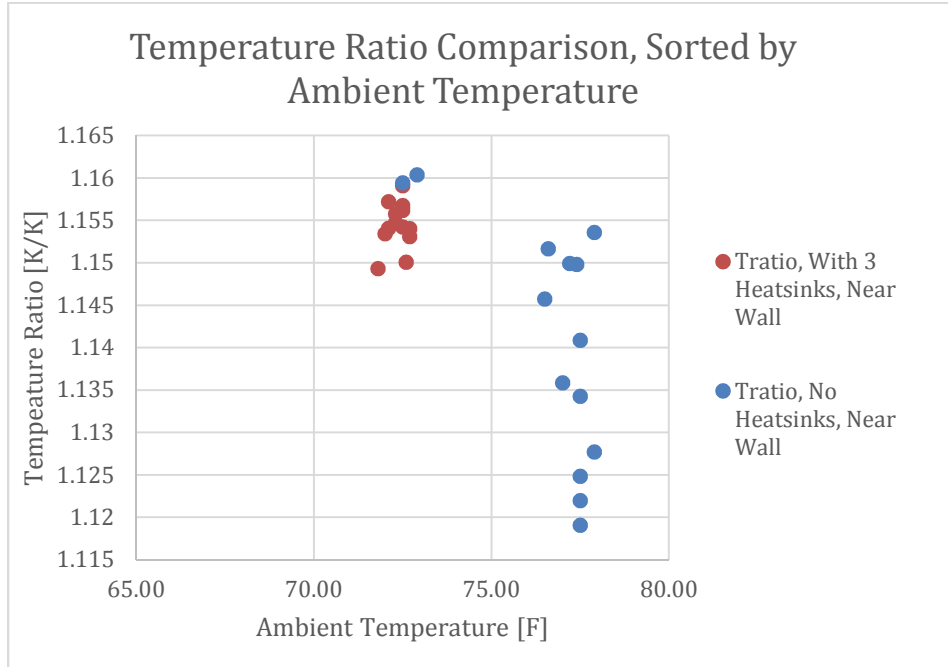
Figure 19. Temperature Ratio, With and Without Heatsinks

A second comparison was made using a unit with three heat sinks attached to the cold plate, the first test conducted near the wall and the other away from the wall. The results are sorted by ambient temperature, and ambient temperature for both test was recorded at a high of about 1.5 feet over the top of the unit. Away from the wall, the temperature ratio was consistently higher than near the wall. Also, near the wall, the unit only ran for a few hours before stopping. Away from the wall, the unit ran for over 24 hours before being stopped. Tests were not conducted in a tightly controlled ambient environment, and there was variance in ambient temperature over the time period.
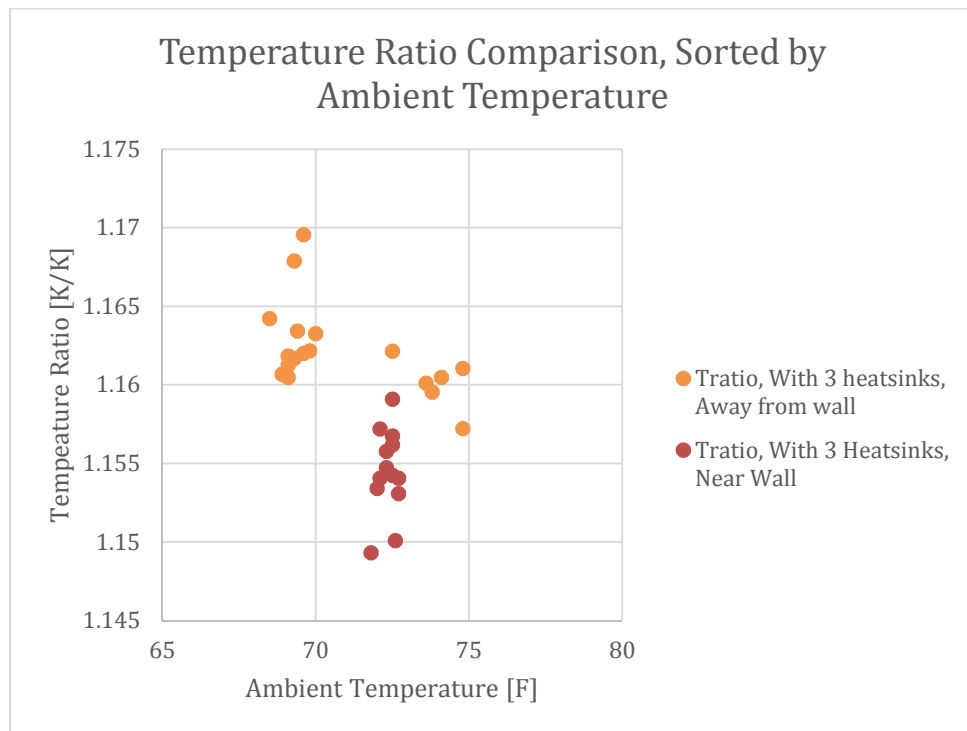

Figure 20. Temperature Ratio, Near versus Away from the Wall

The last test was conducted by adding 10 heatsinks, rather than 3 heatsinks, to see if the additional area made any difference if the unit was against the wall where the natural convection seemed to be less effective than away from the wall. According to Figure 21, even though more heatinks were used, and thus more surface area is added, it doesn't appear to have a noticeable effect.
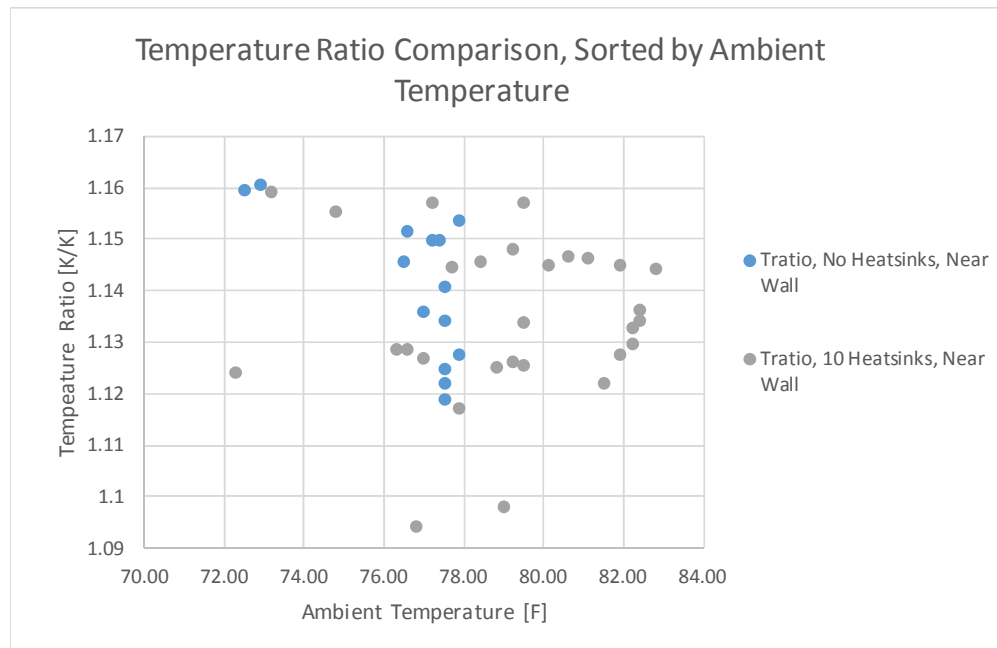

Figure 21. Temperature Ratio Effect of Ten versus No Heatsinks, Near Wall

The conclusion drawn from the cold side heat dissipation test was that while adding heatsinks provided improvement, the proximity to the wall negatively affected natural convection, and could not be overcome with additional heatsinks.

3. Regenerator

The regenerator is a component that extracts thermal energy from the working fluid when it flows from the hot side to the cold side, and returns the heat to the working fluid when it moves back to the hot side. This test was conducted to find out the effect of a regenerator, and determine if it would be beneficial to the performance.

A 53 Watt bulb was installed and a regulator was used to vary the input power to control Hot Plate Temperature. Ice packs were used in some tests to control cold plate temperature. Power In, Temperatures and Rotational speed were recorded for each test point.

The baseline test was conducted without a regenerator. The tests were then repeated with folded fins installed in the regenerator cavity. Each fin had three folds, and two fins were stacked on top of each other in each section.
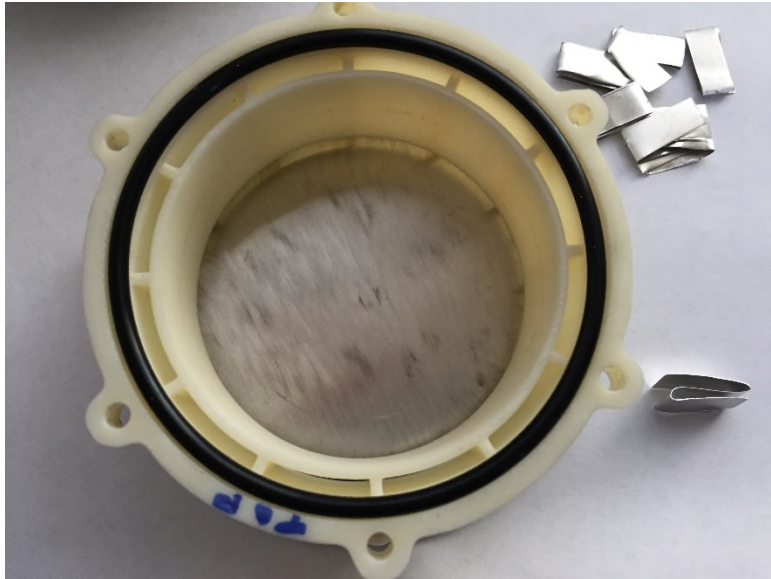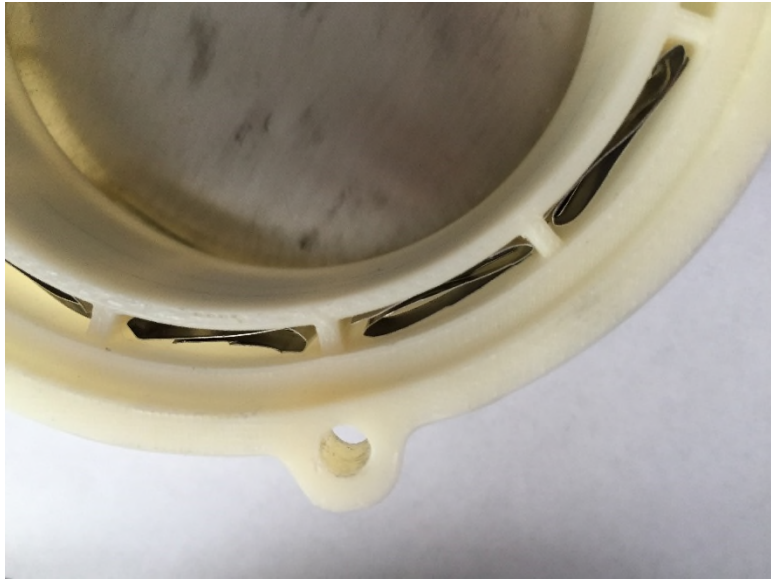
Figure 22. Empty Regenerator

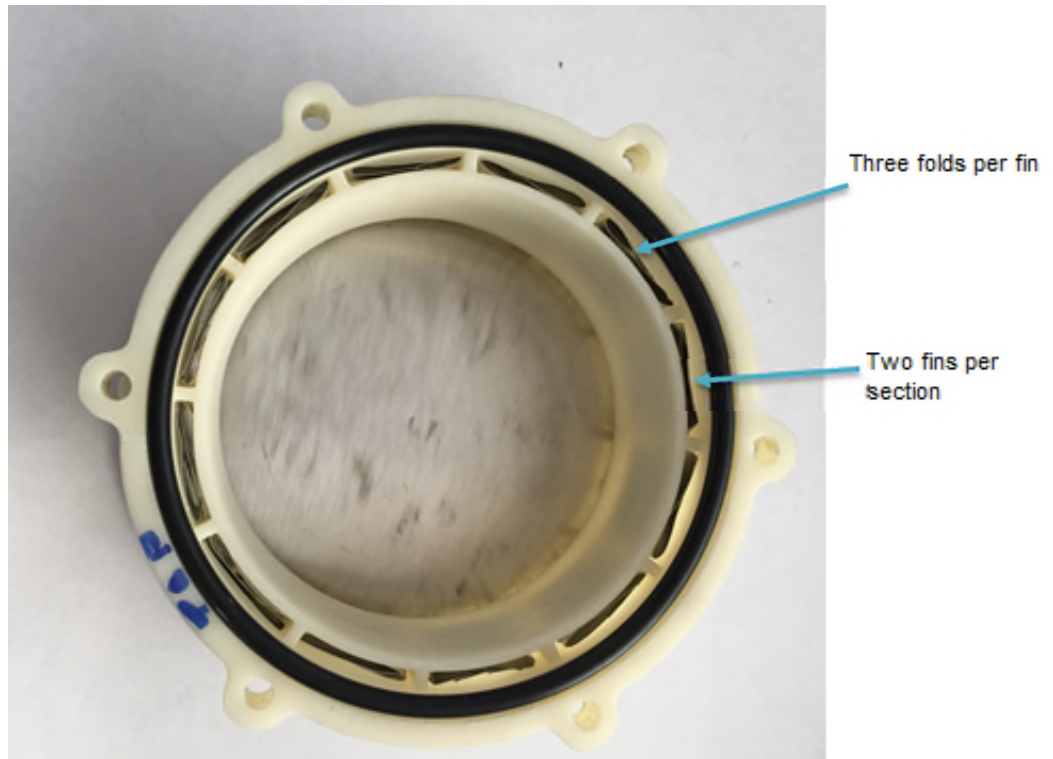Figure 23. Regenerator with Folded Fins, Close-Up

Figure 24. Regenerator with Folded Fins Installed

The results of the testing showed that the rotational speed was faster with the regenerator for each given temperature ratio. The points at the bottom of the graph (Rotation speed = 0 Hz) indicated that the engine stopped on its own, and temperature data was recorded. The regenerator allowed the engine to run at lower Temperature Ratios, however failures at the lower temperature ratios were more common.
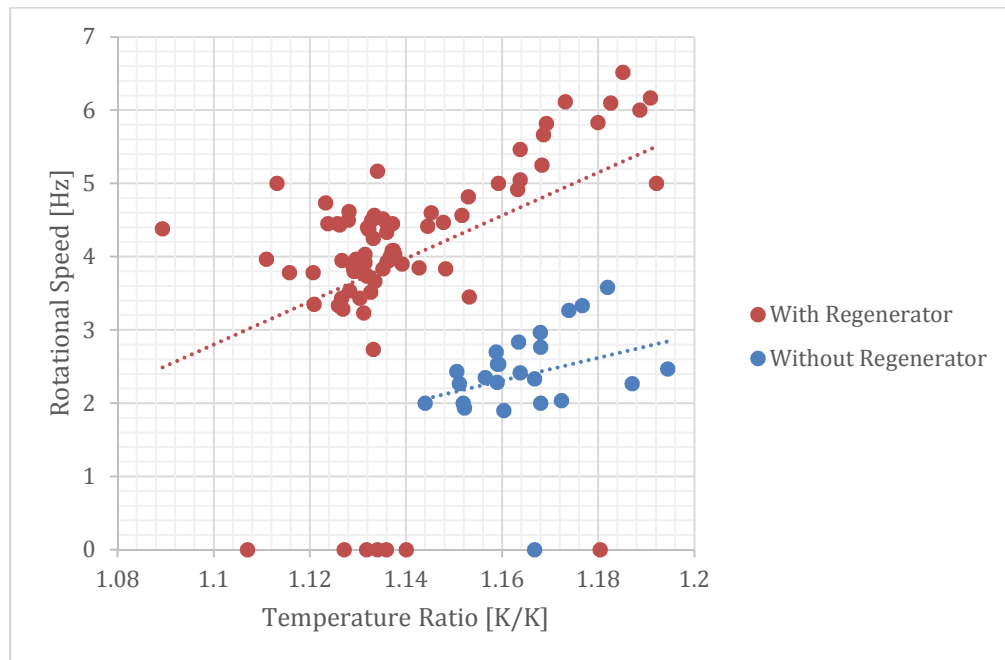
Figure 25. Rotational Speed With and Without Regenerator

Without the regenerator, the engine would run with an average temperature difference between the hot and cold plate of 90.7F, and an average hot plate temperature of 182.3F. With the regenerator, the hot plate was cooler (176.1 F), but the cold plate was hotter (98.2 F), resulting in a measured temperature difference of only 77.9 F. The average temperatures are shown in Table III. These results show that although separate fins were

45

stacked, the regenerator still contributed to axial conduction from the hot side to the cold

side. Increasing the number of layers or using a random-fiber porous material (Ibrahim &

Tew, 2012) may be used in future builds to reduce the axial conduction.

Table III. Average Plate Temperatures With and Without Regenerator

	Without Regenerator	With Folded Fins
Average Hot Plate Temperature	182.3 F	176.1 F
Average Cold Plate Temperature	91.5 F	98.2 F
Average Temperature Difference	90.7 F	77.9F

4. Engine Friction Power Test

By measuring the rate at which friction slows the flywheel's kinetic energy, it can be determined how much power the engine must produce in order to overcome the unloaded engine friction. This test was conducted by separating the hot and cold plates in order to unseal the engine so that compression effect wasn't included. The flywheel, still connected to the power piston and displacer were spun, and the time between flywheel rotations was measured. This was similar to method described by Conner (Conner, Solar Heat Engines, How to measure engine friction using flywheel deceleration, 2013) where he used a Hall-effect sensor and automated data output program to record the passage of a magnet. The slowdown happens very quickly, within just a few seconds, and the tachometer used for steady-state measurements didn't react fast enough to record the changes. Instead, a high speed camera was used to record the slowdown at 240 frames per second.

Kinetic Energy ($KE = I\omega^2/2$) was calculated at using the time it took to complete each pass, and the power lost was calculated by the change in KE at each subsequent point. At least 3 points in time were needed to complete the calculation.

$KE_1 = I\omega_1^2/2$ where $\omega_1 = 2\pi\ (1/(time_2-time_1))$

$KE_2 = I\omega_2^2/2$ where $\omega_2 = 2\pi\ (1/(time_3-time_2))$

Average power loss during the time period is : $Q = 2\ \text{x}\ (KE_1 - KE_2)/time_3-time_1$

The test was conducted on two different Stirling engine configurations, one with the magnet-weighted flywheel and one with the unweighted flywheel. The tests were repeated 3 times on each unit. The Engine Friction Power curves for both units are shown in Figure 26.
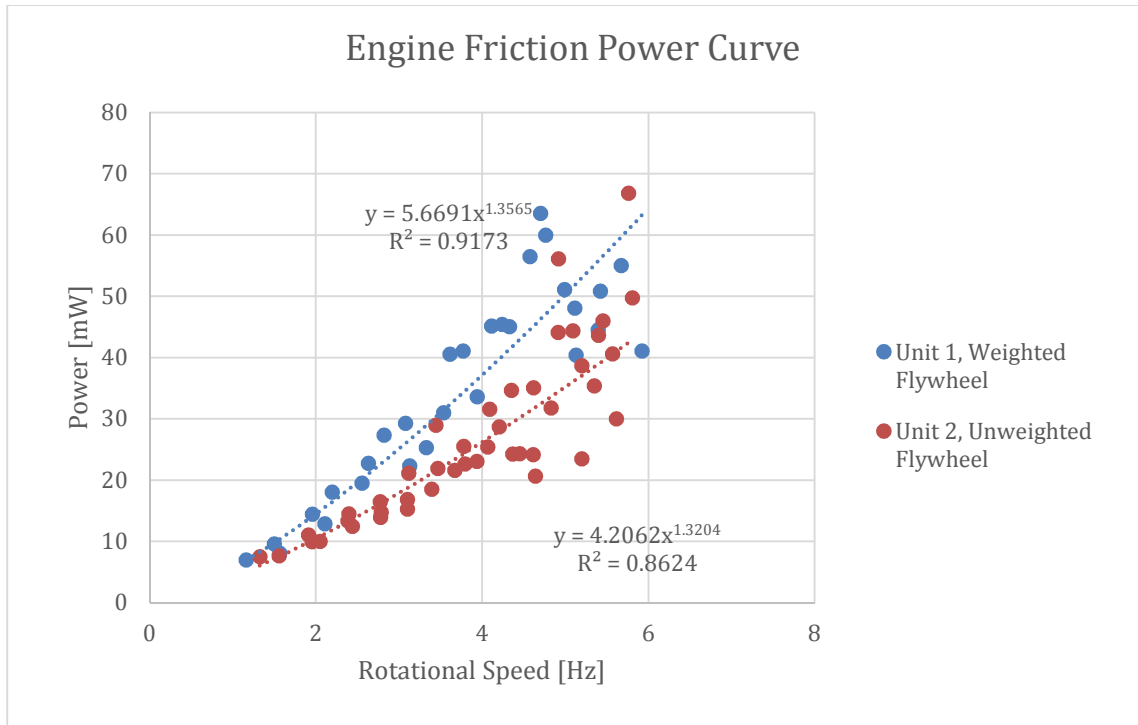

Figure 26. Engine Friction Power Curve

5. Power Measurement Systems

a)   Electromagnetic

The method to measure power output via axial flux did not work out as anticipated. The amount of power that needed to be applied to the circuit to stop the rotation was much higher than expected. The resistance shunt was removed and the magnets were rearranged so that all the poles faced one direction to try to increase the braking power, but the amount of power needed was still too much for the coils and they would get very hot. It was not possible to apply the power continuously for more than a few seconds. Power was pulsed on to try to gauge response, then adjusted and pulsed on as needed. Readings were obtained and recorded when possible, but don't appear to be consistent.

The figure below shows the Temperature ratio versus Braking Power for the points that were obtained. Results do show a trend, but with several outliers.
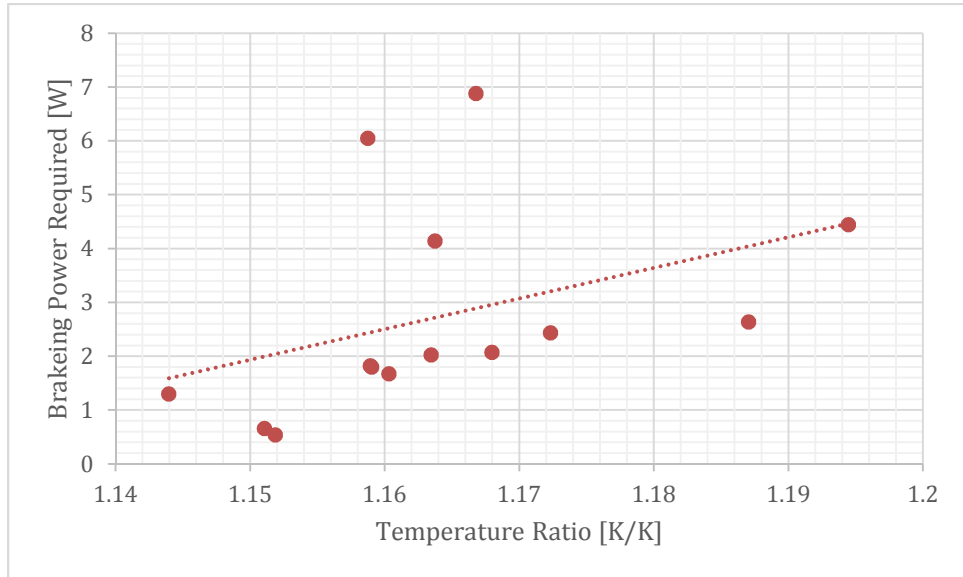

Figure 27. Temperature Ratio versus Braking Power Required

Results were more than two orders of magnitude higher than analysis. The test scale is on the left vertical axis, and analysis scale on the right vertical axis. Since the linear slopes of the lines don't appear to be the same, a linear calibration is not applicable.
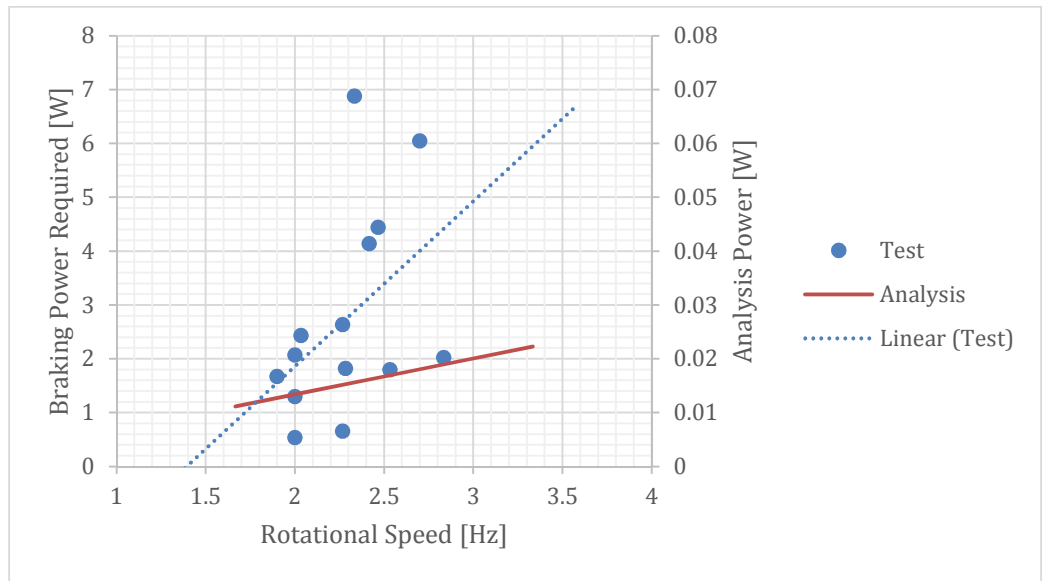

Figure 28. Measured Power Results versus Analysis

An attempt was also made to try to measure power generated by the flywheel passing by the coils, instead of applying current to the coils. A multi-meter was used to try to measure voltage and current at the shunt, but no readings were detected.

b)   Lifting a Weight Against Gravity

The second method to measure the output power was developed based on the time it takes to raise a known weight over a measured distance. As described in Chapter IV, the Stirling engine was fitted with a spool. The spool would wind a thread with a calibration weight attached. The Stirling engine flywheel was spun up by hand to start it, and the and the spool would begin to wind thread from a reservoir loop, or slack in the thread, so the initial spin of the flywheel would not factor into the result. A poster to mark the units of length was displayed behind the weight, and a camera was used to record the motion.

Input power was 39 Watts and it reached a temperature ratio of 1.13 and a flywheel speed of 2.5 Hz. The test was conducted 5 times in order to get multiple data points. For the five different tests, the weight would rise between 10mm and 90mm. It's unclear from the data or the video footage what causes the stops at different heights. Using average speeds of the raising of the weight over the test runs (1.57 seconds per 10 cm) the output power is approximated at 3.1 mW.

The string was wound onto a spool approximately 15mm in diameter. The spool was mounted to a linkage near the center of the wheel. The power measurements recorded by Conner were made at the outer diameter of the flywheel, which is 145mm in diameter. Measuring at the out edge of the flywheel would be expected to add a mechanical advantage due to the increased diameter. Because of the location of the linkage and proximity of the wheel to stationary parts on the engine, it was not readily feasible to spool

wire on the outer diameter of the wheel using the current design. As shown in Figure 29, anything on the wheel need to pass between the flywheel and the piston, or between the flywheel and the stand.
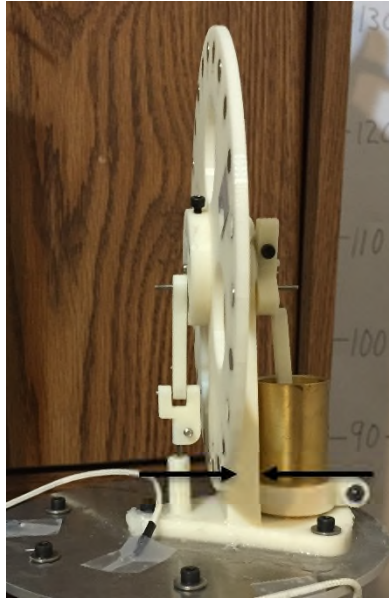

Figure 29. Space between Flywheel and Piston

Based on the circumference of the spool, the engine was able to pull the weight at an average speed of 1.355 cycles per second. If it is possible to extrapolate that to the circumference of the flywheel (45.5 cm), it translates to a rate of 0.616 m/s, which would result in a power output measurement of 30.2 mW. This is just an estimate, as actual response of the system would have to be verified.

The value of 3.1mW is considered the net output of the unit. In the next section, net power output will be used to calculate the 1st and 2nd order efficiency of the engine. Adding net power output to the result of the friction test equals the gross power output. Gross power output can be compared to the results of the analysis predictions.

6. Power Output Analysis and Comparison to Test Results

As described in Chapter II, there are analysis methods that could be applied to the Stirling engine specifications to estimate power output. The Beale Equation was an example of a first-order method for power estimation, and was used to calculate the power expected from the 3D printed Stirling engine. The results are shown below.
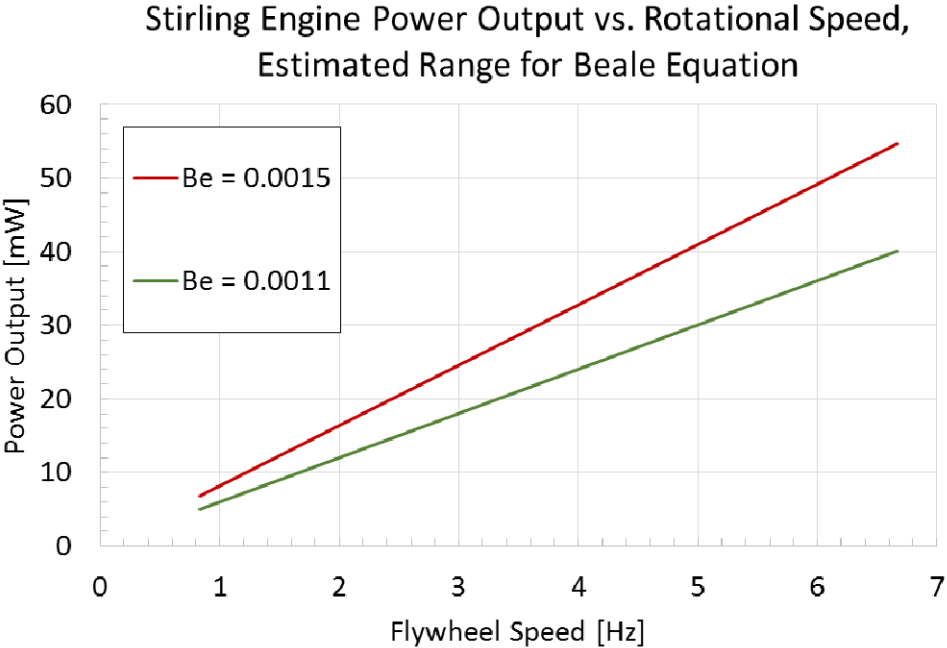
Figure 30. Beale Method Prediction of Engine Power

Using Martini's method for isothermal analysis, a second prediction for the output of the 3D printed Stirling engine was calculated. This is a second-order analysis, where a simplified cycle analysis is used to determine basic power output and heat input. Pressures and volumes are calculated at incremental phase angles of a cycle. The results are then integrated over the cycle to calculate work output.

54

Based on the dimensions of the engine, and using hot and cold Temperatures of 350K and 303K, respectively (170F and 85F), the resulting output is shown in the graphs below.
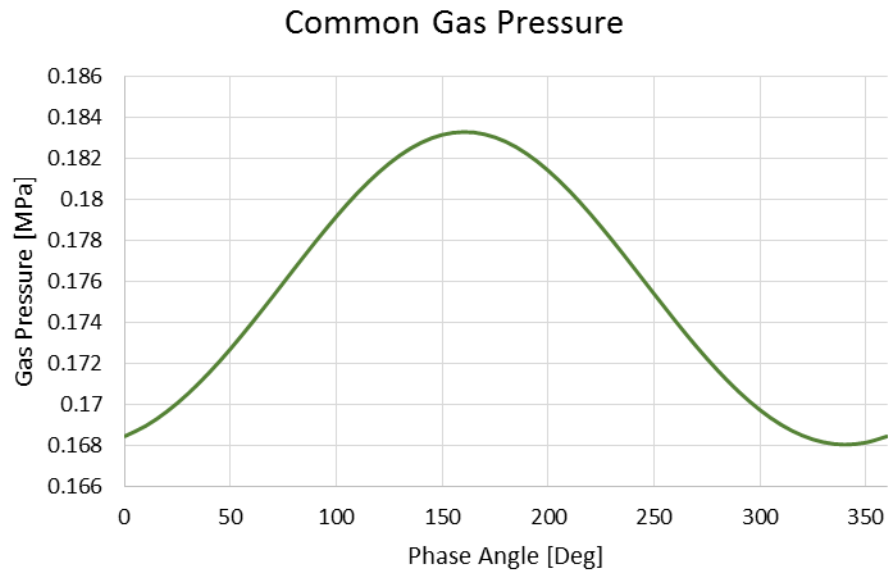
Common Gas Pressure

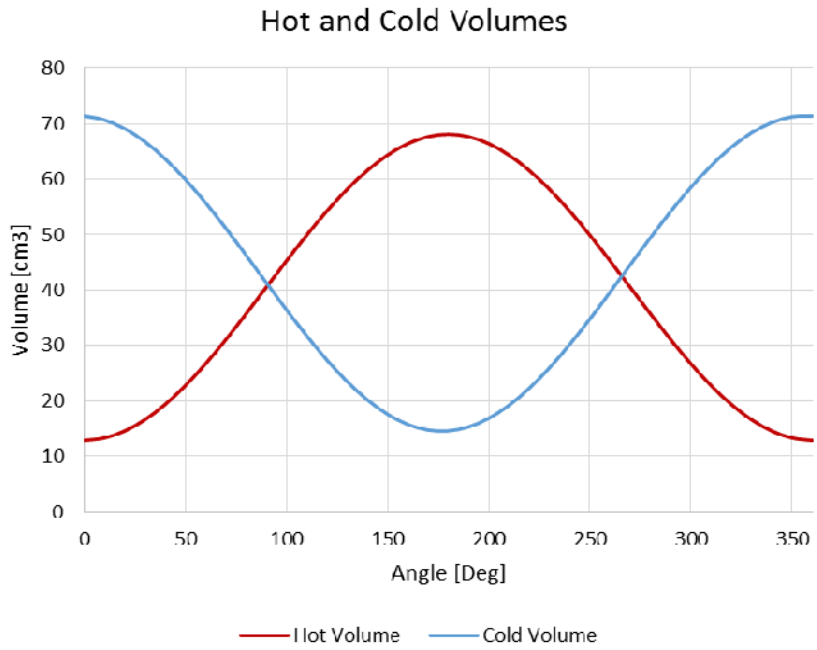Figure 31. Common Gas Pressure through One Cycle

Figure 32. Hot and Cold Volume Pressures through One Cycle
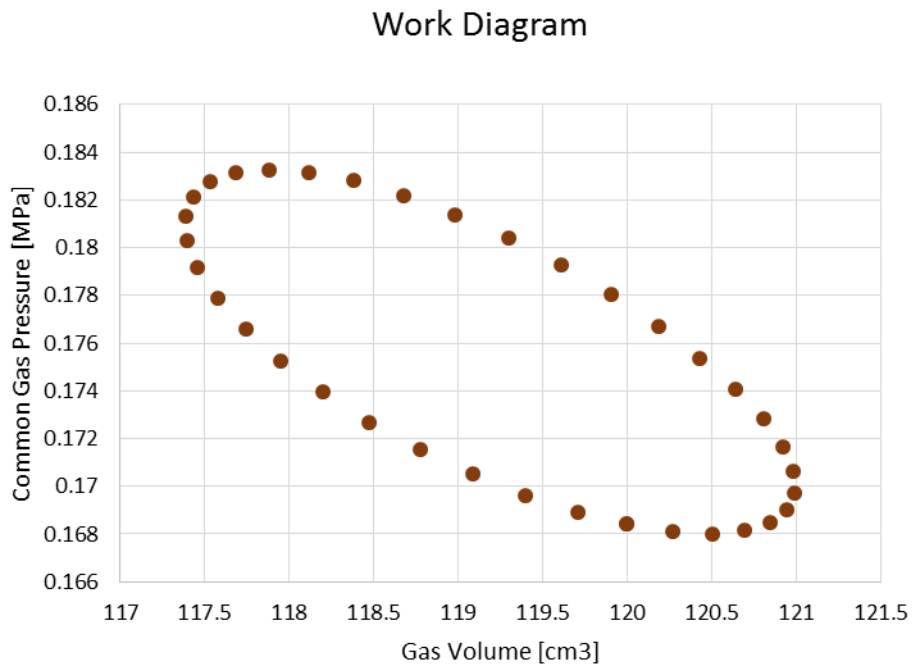
Figure 33. Work Diagram through One Cycle

56

The work produced during one cycle of the 3D printed Stirling engine is calculated in joules/sec, and the power output is then dependent on the speed of the engine. The figure below shows this linear relationship.
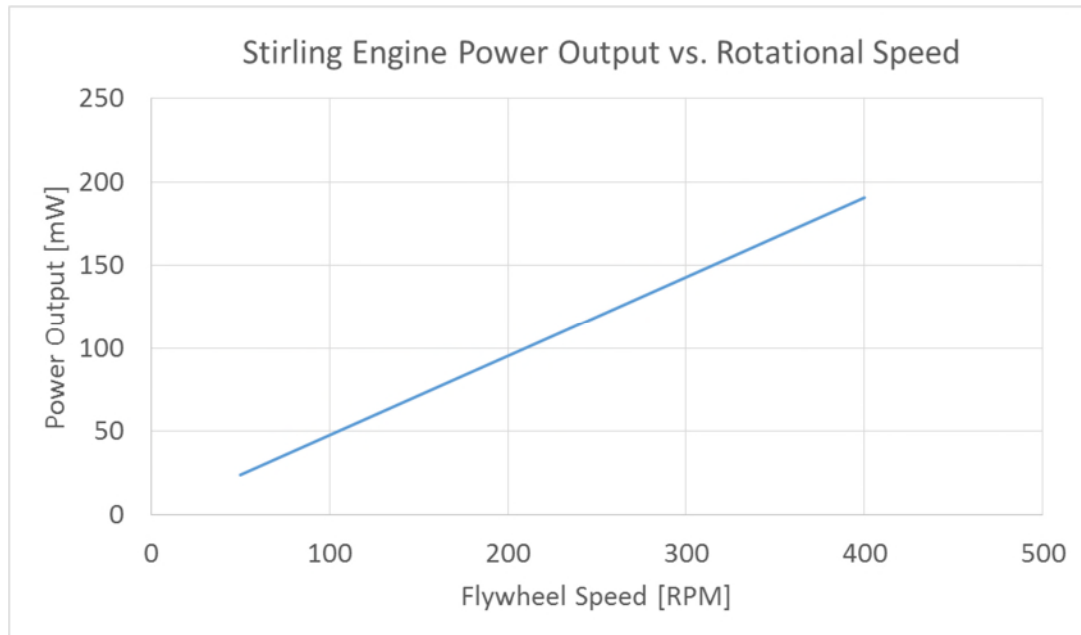
Figure 34. Stirling Engine Power Output versus Rotational Speed

Since there is a limited temperature range for the 3D printed Stirling engine, there wasn't much variation in experimental temperature ratio. To illustrate this relationship the same isothermal analysis was conducted using a hot side temperature of 350K (170F), and cold side temperatures of 310K (98F), 303K (85F), 294K (70F), 287 (57F) to create temperature ratios of 1.13, 1.17, 1.19 and 1.22, respectively. The results of this analysis are shown in Figure 35. As demonstrated by the figure, limited by the temperatures reasonable

for this unit, varying temperature ratios will not provide significantly different power results.
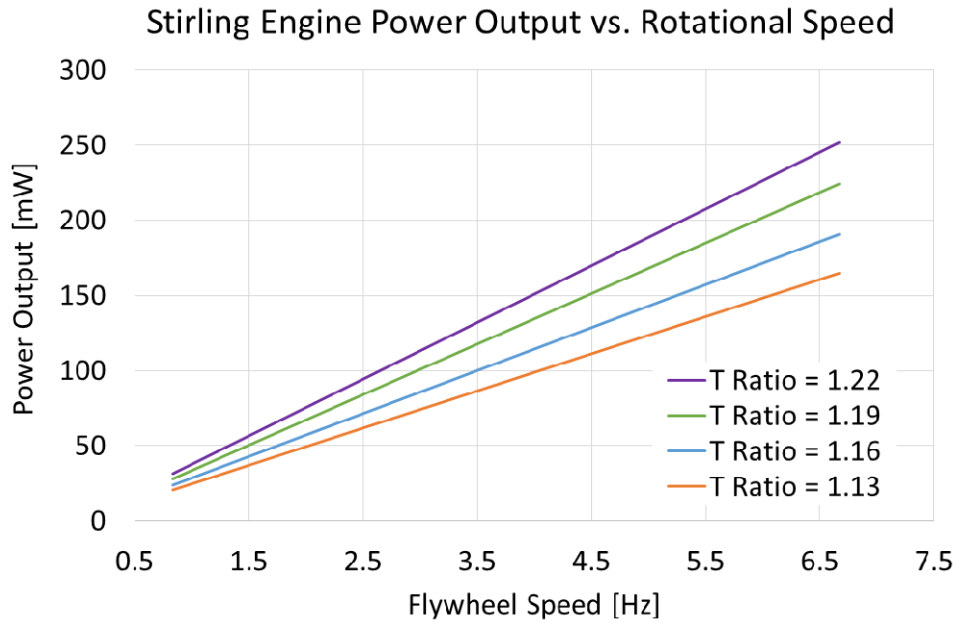
Figure 35. Analysis Results Varying Temperature Ratio

The results of the two analysis methods yield relatively different results. The Schmidt isothermal analysis prediction is 3-5 times higher than the Beale estimation over the expected operating range.
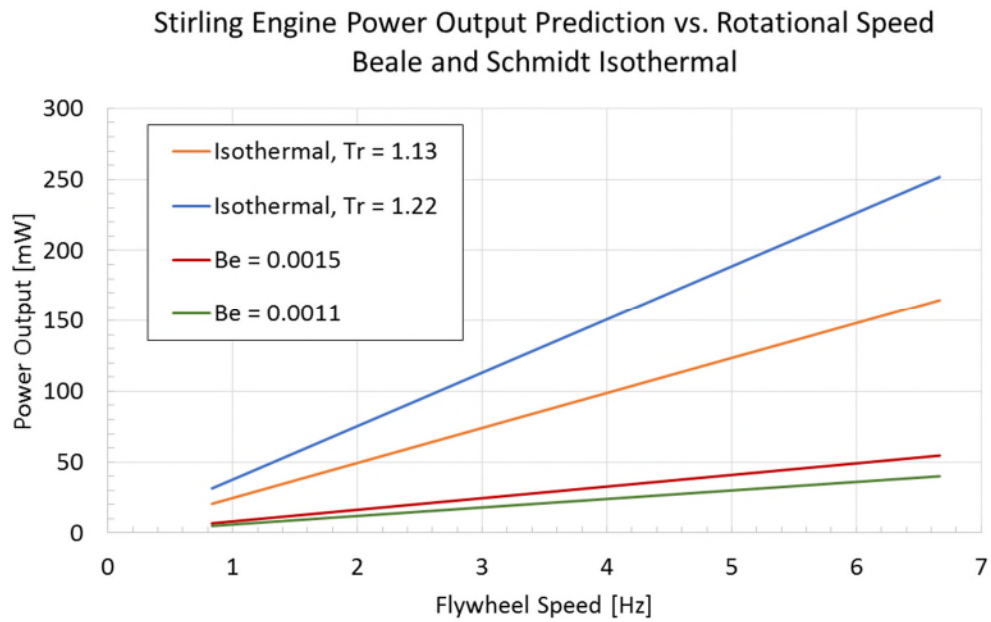
Figure 36. Comparison of Beale and Schmidt Isothermal Analysis Results

The results of the analysis using can also be compared to the test results supplied by Connor (Conner, Solar Heat Engines, Power output measurement of the PE 2 Stirling engine, 2013). Conner conducted series of tests where he measured the net output of the engine and engine friction and used it to derive gross power output. According to Conner, the gross output power is the sum of the measured net power output and engine friction losses. Conner measured net power at multiple rotational speeds, but it was nearly constant between 2.5 and 4 Hz. The results closely corresponded to a Beale number of 0.0015. The Isothermal analysis prediction for gross power at the same temperature ratio was more than 4 times higher and is not shown in the graph.
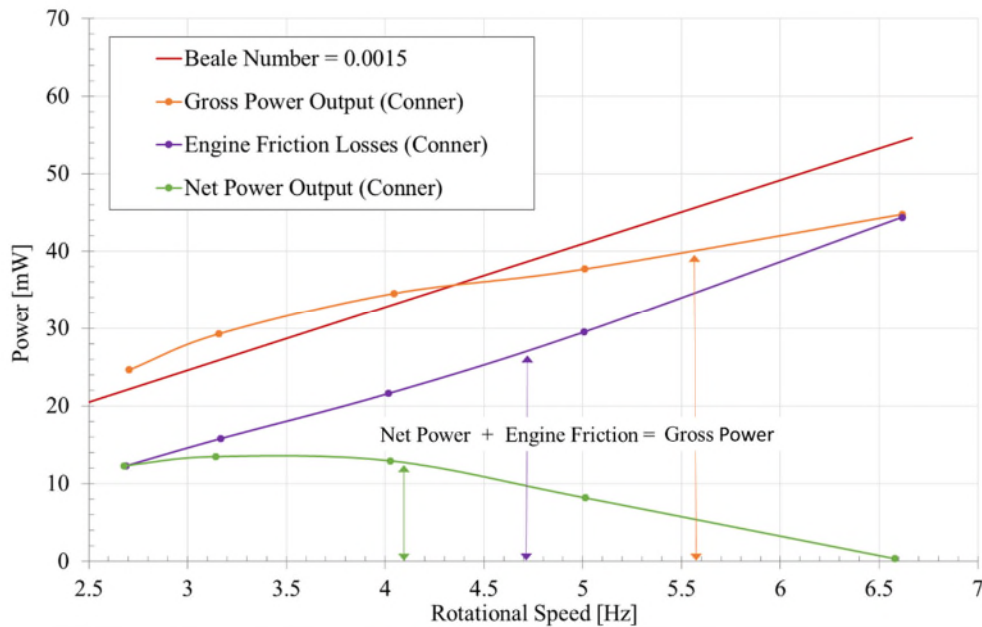
Figure 37. Comparison of Analysis to Previous Testing on Similar Engine

60

Figure 38 shows the results of the net power and engine friction power tests that were conducted as part of this thesis. Net power and engine friction are also combined to account for the gross power of the engine. Net power was measured at one rotational speed, but assumed to be constant up to 4 Hz. Also shown is the results of the the Beale analysis and the Schmidt isothermal analysis (using a Temperature Ratio of 1.13). The gross power output corresponded to a Beale number of approximately 0.00125. The second order analysis prediction was about 3.5 times higher than the test results.
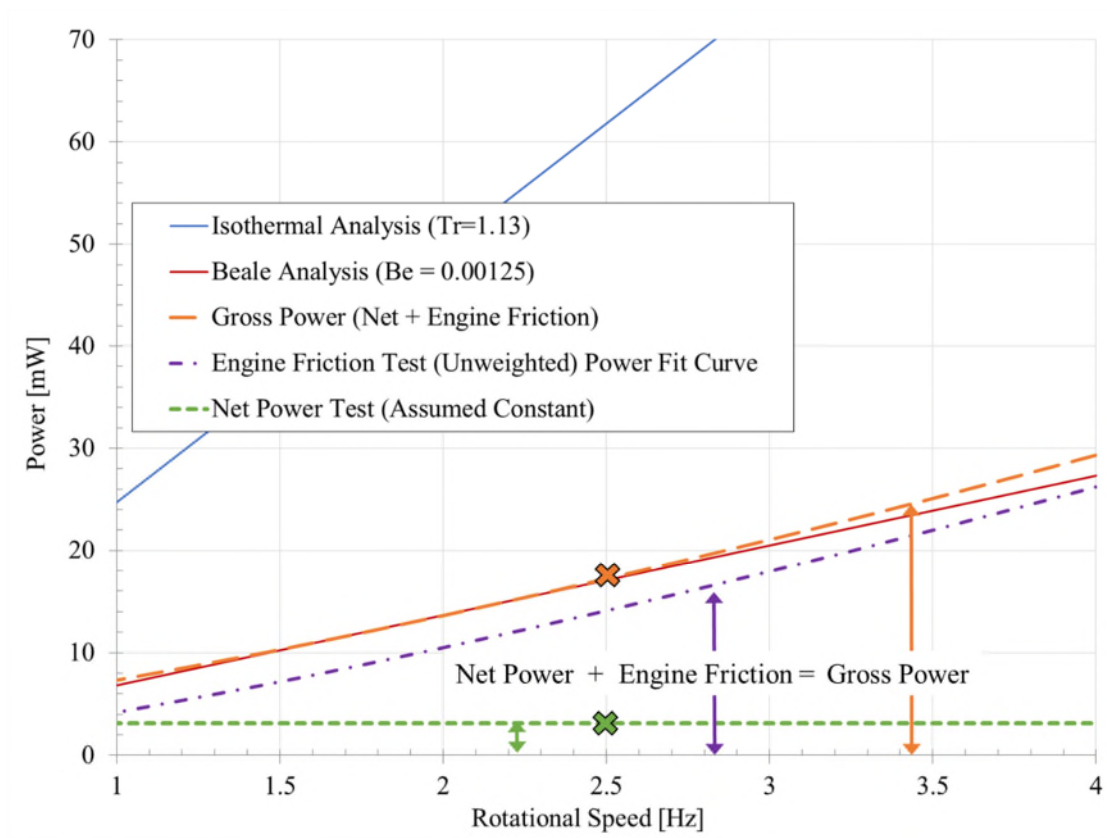
Figure 38. Comparison of Output Power Testing and Analysis Predictions

B. EFFICIENCY CALCULATIONS

The maximum efficiency of a Heat Engine will be Carnot. This engine was tested with a hot side temperature of 168 °F (349 K) and a cold side temperature of 94 °F (308K). Using these parameters, Carnot Efficiency is 11.7%.

$$\eta_{Carnot} = \frac{T_{Hot} - T_{Cold}}{T_{Hot}} = \frac{349K - 308K}{349K} = 11.7\%$$

According to the Carlqvist Formula (Martini, 1983), a first order analysis method for Stirling engines, for an optimized engine, 58% of Carnot should be expected.

$$\eta_{Carlqvist} = \eta_{Carnot} * 0.58 = 6.8\%$$

Thermal efficiency, also referred to as 1st Order Efficiency, is calculated using the equation

$$\eta_{1st\ Law} = \eta_{th=} \frac{Q_{net}}{Q_{in}}$$

According to power output data which was a net of 3.1mW, the thermal efficiency of the system was about 0.0079%, was much lower than the Carlqvist estimate.

$$\eta_{th=} \frac{Q_{net}}{Q_{in}} = \frac{0.0031\ W}{39\ W} = 0.0079\%$$

Another way to quantify of thermodynamic availability is by using the concept of 2nd Order Efficiency. This is described as the actual output of the engine divided by the decrease in availability, or how much of the theoretical maximum can be achieved. Second law efficiency should fall between Carnot and 1st Law efficiency, and can be calculated by dividing the thermal, or first law efficiency, by the Carnot Efficiency.

$$\eta_{2nd\ Law} = \frac{\eta_{th}}{\eta_{Carnot}}$$

For this engine, the second law efficiency is calculated to be 0.068%

$$\eta_{2nd\ Law} = \frac{\eta_{th}}{\eta_{Carnot}} = \frac{0.000079}{.117} = 0.068\%$$

C. LOSSES, ISSUES AND FIXES

If a Stirling engine runs, losses can be tracked and addressed. However losses can be such that the engine won't run at all, making the process much more difficult. (Shelton, 1994). This turned out to be an obstacle for this thesis.

One of the first issues is that without active cooling, the cold side quickly heats up and reduces the temperature difference, which is necessary to operate. One issue identified was the thermal path created by the screws that connect the hot plate and cold plate to the cylinder in the original design. An option to eliminate this path was to use separate screws for the hot plate and cold plate.

Figure 39. Original Plate Attachment
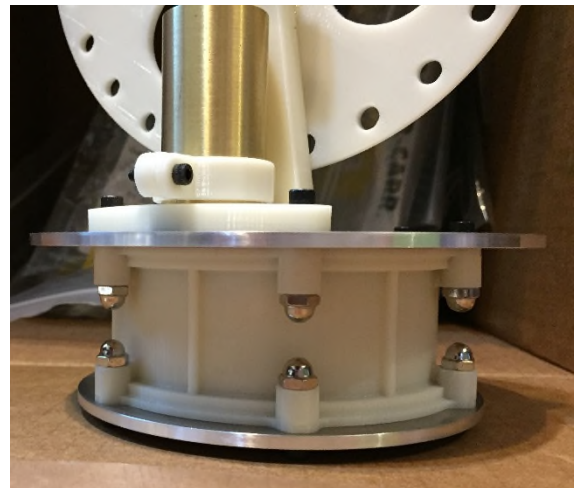
Figure 40. Revised Plate Attachment

While the mounting method appeared to help initially, operation again deteriorated over time. The first prototype was powered with a 39 W bulb. Adding more heat in the form of a higher wattage bulb would make it run, but the increases were pushing the boundaries of the acceptable temperature for the ABS plastic. Also, without active cooling, the cold side heat exchanger was unable to dissipate the large amount of heat applied, and the temperature difference would continue to shrink. Eventually it became apparent that even at the higher heat input, it was not generating the pressure needed to move the pistons for even a short amount of time. After inspection of one of the units, cracks were discovered in the regenerator cylinder.

Although the separate screws did reduce the thermal path, they created a structural issue. In order to seal the unit, and the screws compress O-rings between the plates and the cylinder. Fused deposition modeled parts such as this one, which was built from the bottom to top, is strongest in compression, and weakest in tension along that axis (Smyth, 2014). When separate screws were used, compressive stress changed to tensile stress on the cylinder, causing cracking around the mounting feet of the cylinder.

Figure 41. Cracking Around Hot and Cold Plate Mounts

After silicone adhesive was liberally applied around the sides of cylinder to seal the

leaks, the engines resumed operation. On one of the units, longer screws put back into the

assembly, but with fiber washers between the plates and the metal washers to reduce the

thermal path.
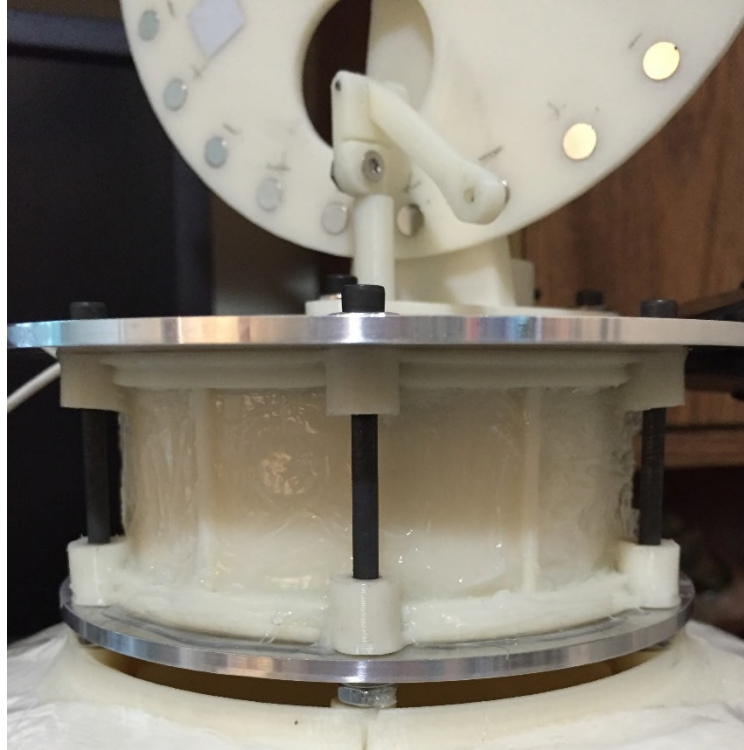
Figure 42. Cylinder Repaired with Silicone

Another option to remedy the cracking would be to re-design the cylinder to create ribs near the engine mounts to add structural integrity. This may be incorporated in a future build.

Mechanical friction was also a problem that contributed to the engine stalling. When working with moving parts, some friction is normal or unavoidable, but the 3D printed engine included some unique issues. One example was the displacer and power pistons making contact with their respective cylinders. The outer diameters of the piston and inner diameters of the cylinder were designed to be close without touching. Maintaining the tolerance around the circumference was difficult for both, particularly for

the displacer piston which was cut from foam, and the 3D printed cylinder. Both the foam piston and the 3D printed cylinder were not perfectly round, and when aligned in certain clocking angles would touch and cause friction. If the metal rod holding the displacer piston become bent even slightly, the piston would rub against the cylinder wall.

The flywheel itself was also slightly out of round, and would occasionally strike the pedestal that held it. Material was removed from the pedestal to minimize the change of contact, but the motion caused by the flutter of the flywheel would cause the parts to walk, and contact between the flywheel and the pedestal, or other plastic parts in the assembly would cause the engine to stop.

It was learned that friction and air leaks are key factors in hindering operation, but can be tested each time the engine is started. Friction was checked by removing the power piston linkage from the flywheel, and spinning the flywheel. It should spin freely with no sound from the displacer piston or from the bearing assembly. To test for air leaks, the power piston can be held at the top of the cylinder, and allowed to drop. Because the unit should be nearly air tight, it should drop very slowly against internal pressure and take over 10 seconds to reach the bottom.

Although not considered a major contributor, fluid friction could also account for losses. The transitions in the air path included sharp bends and sudden expansions, and would benefit from flow analysis and optimization.

The lamp base, designed primarily to display an illuminated logo, allows light and heat to escape, and is not optimized for efficiency. An insulated base would allow a much lower watt light bulb to attain the same hot side temperature.

In order to quantify the amount of actual heat that is applied to the engine, a test was conducted to measure the time rate of change of temperature in the hot plate when heated with the 39 Watt bulb.

$$Power_{Actual} = \frac{m \times C_p \times (\Delta T)}{t}$$

where

   m = mass of the plate, 87 g

   Cp = specific heat of aluminum, 0.875 J/g *K

   ΔT = change in temperature, K

   t = time, seconds

The aluminum plate was weighed to determine the mass.   Three thermocouples were attached to the plate. Styrofoam insulation was placed over the plate to reduce heat loss.

Figure 43. Actual Power Input Test

After 10 minutes, or 600 seconds of applied heat, the temperature of the plate rose from 287.5 K to 318.4K. This corresponds to an actual power input of 3.9 Watt, or about 10% of the power input of the bulb.

The efficiency can be recalculated based on the revised power input, and is now an order of magnitude higher than the previous estimate.

$$\eta_{th=} \frac{Q_{net}}{Q_{in}} = \frac{0.0031\ W}{3.9\ W} = 0.079\%$$

$$\eta_{2nd\ Law} = \frac{\eta_{th}}{\eta_{Carnot}} = \frac{0.00079}{.117} = 0.675\%$$

D. HEATSINK OPTIMIZATION

It has been demonstrated by testing on the Stirling engine that the presence of heatsinks can affect the heat transfer. Heat sinks are frequently used in electronics cooling to transfer heat from the device to the heat sink via conduction, and from the heat sink to the ambient air via natural or forced convection. The amount of heat that can be transferred from the cold side to the ambient air is governed by the following equation.

$$q = h_c \, A \, (T_s - T_\infty)$$

where q = heat transferred per unit time

A = heat transfer area of the surface

h_c = convective heat transfer coefficient

T_s = Cold plate surface temperature

T_∞ = Ambient temperature

While increasing the number and size of the heatsinks increased the area (A) available for heat transfer, another factor is the spacing of the fins.

The convective heat transfer coefficient (h_c) is proportional to the flow rate of the fluid. Forced convection typically employs a fan to increase the flow rate of the fluid. In most applications, including ours, natural convection is preferred since it requires no moving parts (Cengel & Ghajar, 2011). The key to optimizing natural convection is balancing the buoyancy forces of the warm air with the friction forces of the solid surfaces. As observed during testing with the unit near a wall, the friction forces of the warm air near

71

the wall reduced the heat transfer. The same phenomenon is applicable to the heatsinks themselves. The buoyancy force on the fluid moving along a heatsink fin can be slowed by the friction force of the adjacent fin. In a forced convection application, the flow can be high enough to overcome this friction force, and higher density fins are appropriate. However, for a natural convection application, a wider spaced heatsink is needed, and a properly sized heatsink is imperative for reliable operation. (Cengel & Ghajar, 2011)

A dimensionless parameter call the Grashoff number, Gr is used to quantify the relationship between buoyancy and viscosity within the fluid. (Cengel & Ghajar, 2011).

$$Gr = \frac{g \, \beta \left(T_{surface} - T_{ambient} \right) L^3}{v^2}$$

where

g = gravitational acceleration [m/s^2]

β = coefficient of volume expansion [1/K]

h_c = convective heat transfer coefficient

$T_{surface}$ = temperature of the heat sink surface [K]

$T_{ambient}$ = fluid temperature, sufficiently far from the surface [K]

L = characteristic length of the geometry [m]

v = kinematic viscosity of the fluid [m^2/s]

The Grashoff Number and the Prandtl Number, Pr, which is describes the relative thickness of the velocity and thermal boundary layers in a fluid, are used to find the Rayleigh Number, Ra. The Rayleigh number is used to characterize the transition of free

convection boundary layer flow from laminar to turbulent. For a vertical finned heatsink, the Rayleigh number can be expressed in terms of the spacing between fins Ra_s, or in terms of fin height, Ra_L

$$Ra_S = \frac{g\beta(T_s - T_\infty)S^3}{\nu^2} Pr$$

$$Ra_L = \frac{g\beta(T_s - T_\infty)L^3}{\nu^2} Pr = Ra_S \frac{L^3}{S^3}$$

In order to optimize spacing, the equation Ra_L is used and the height of the fin, L, is known. The heatsink used in this application has fin heights of 12mm and 13mm.
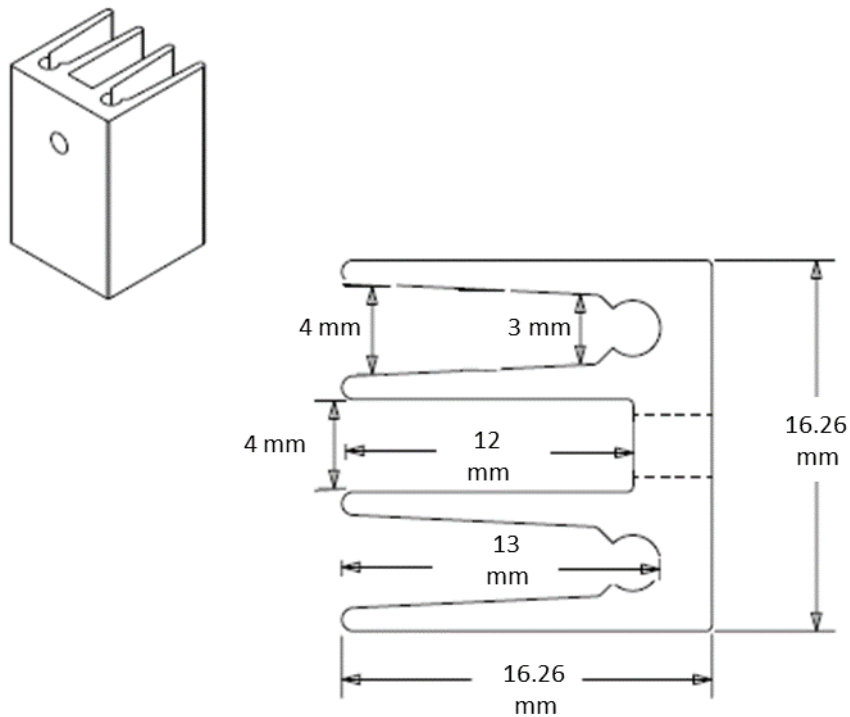

Figure 44. Heatsink Dimensions

Ra$_L$ for the application can be calculated using the following properties:

Film Temperature = T$_f$ = (T$_s$ +T$_\infty$) / 2 = (310K + 299K)/2 = 304.5K = 31.35 C

$g = 9.81$ m/s^2

$k = 0.02598$ W/m K

$v = 1.621$ x10^{-5} m^2/s

$Pr = 0.7278$

$\beta = 1/T_f = 1/304.5$ K

(T$_s$ -T$_\infty$) = 11K

L=12mm and 13mm = 0.012 m and 0.013 m

First for 12mm,

$$Ra_L = \frac{\left(9.81 \ \frac{m}{s^2}\right) \times \left(\frac{1}{304.5K}\right) \times (11K) \times (0.012)^3}{\left(1.621 \times 10^{-5} \ \frac{m^2}{s}\right)^2} \times (0.7278) = 1696.15$$

The Optimum Spacing then can be determined by the following equation

$$S_{OPT} = 2.714 \ \frac{L}{Ra_L^{0.25}} = 2.714 \frac{0.012m}{(9.825 \times 10^{\wedge}8)^{.25}} = 5.07 \times 10^{-3}m = 5.07mm$$

The calculation was repeated for 13mm to obtain a Ra$_L$ = 2156.5 and an optimum spacing of 5.18mm. This optimal spacing is larger than the current spacing (3-4mm), meaning the buoyancy may be hampered by friction forces, and the heatsink is not ideal for this application. The heat transfer would be improved by using optimized heatsinks.

CHAPTER VI

CONCLUSION & FUTURE WORK

The purpose of this thesis was to build a Stirling engine primarily out of 3D printed parts, develop a method to measure the output power, test the performance and compare to analysis results, and determine if adding a regenerator had any effect. Another goal was to identify the obstacles to long term reliability and determine methods to remedy if possible.

While the 3D printed materials turned out to be challenging in sustaining a robust design, the basic operation as a Stirling engine was confirmed. Because of the ease and speed of 3D printing, replacement parts, new designs and design changes were able to be printed and tested quickly.

The power output was measured and confirmed operation similar to analysis predictions. Using at a hot plate temperature of 168F and a cold plate temperature of 94F with a rotational speed of 2.5 Hz, the net power output was measured to be 3.1mW. Adding that to the losses attributed to engine friction resulted in a gross power out of 17mW, which was close to the analysis prediction of 15mW under the same conditions. Estimations for

1st and 2nd order efficiency were also calculated. Efficiency was very low, almost three orders of magnitude lower than an optimized engine, but wasn't a priority for this design. Losses were identified and changes could be implemented to increase efficiency.

Increasing input power increased temperature ratio, but the maximum is capped by the temperature limit of the plastic parts and the lack of active cooling. Using a regenerator did increase the operating speed, but also moved more heat from the hot side to the cold side over time, reducing the temperature ratio and increasing the temperature of the cold plate beyond the capability to be cooled by natural convection.

Increasing the cold side heat transfer to ambient would be one of the most effective factors to increasing reliability. Calculations were made to find the optimal heatsink spacing and compare to the heatsinks used in testing. For future designs, custom heatsinks could be used that maximize the natural convection of the cold side, or a method developed to provide active cooling.

In addition to heat transfer, design changes could be implemented that minimize the dead volume in the regenerator, the hot space and the cold space. Modifying the height of the displacer piston to eliminate any unnecessary space may be beneficial, and perhaps allow expansion of the air to move the displacer at a lower temperature. Reducing fluid friction and optimizing regenerator flow, including consideration of a variable diameter regenerator, is also possible with the capabilities of 3D printing.

BIBLIOGRAPHY

Campbell, T. A. (2013). Additive Manufacturing as a Disruptive Technology:

    Implications of Three-Dimensional Printing. *Technology and Innovation, Vol 15*,

    67-79. doi:10.3727/194982413X13608676060655

Campbell, T., Williams, C., Ivanova, O., & Garrett, B. (2011). Could 3D Printing Change

    the World? Technologies, Potential, and Implications of Additive Manufacturing.

    Atlantic Council Strategic Foresight Report. Washington DC.

Cengel, Y. A., & Ghajar, A. J. (2011). *Heat and Mass Transfer.* New York: McGraw-

    Hill.

Chen, N. C., & Griffin, F. P. (1983). *A Review of Stirling Engine Mathematical Models

    (Report No. ORNL/CON-155).* Oak Ridge, TN: Oak Ridge National Laboratory.

Conner, D. (2013, February 17). *Solar Heat Engines, How to measure engine friction

    using flywheel deceleration*. Retrieved May 28, 2015, from

    http://www.solarheatengines.com/2013/02/17/how-to-measure-engine-friction-

    using-flywheel-deceleration/

Conner, D. (2013, March 15). *Solar Heat Engines, Power output measurement of the PE

    2 Stirling engine*. Retrieved May 28, 2015, from

    http://www.solarheatengines.com/2013/03/15/power-output-measurement-of-the-

    pe-2-stirling-engine/

Egea, A. (2013, January - June). Design of Electric Machines: Axial Flux Machines. *Mondragon Unibersitatea Electric Energy Magazine*, pp. 2-13. Retrieved from http://www.mondragon.edu/en/phs/research/research-teams/electrical-energy/electric-energy-folder/newsletters/no-4-january-june

Gates, B., & Gates , M. (2016, 2 22). *Gatesnotes, 2016 Annual Letter*. (Disqus) Retrieved 2 25, 2016, from https://www.gatesnotes.com/2016-Annual-Letter?WT.mc_id=02_22_2016_00_AL2016_GL-GN_&WT.tsrc=GLGN

Ibrahim, M. B., & Tew, R. C. (2012). *Stirling Converter Regenerators.* Boca Raton, FL: Taylor & Francis Group, LLC.

Lipson, H., & Kurman, M. (2013). *Fabrication, The New World of 3D Printing.* Indianpolis, IN: John Wiley & Sons.

Martini, W. R. (1983). *Stirling Engine Design Manual, 2nd Ed.* NASA/DOE NASA-CR-168088.

Modeling DC Motor Position. (2014, December 9). (National Instruments) Retrieved March 23, 2016, from http://www.ni.com/tutorial/6859/en/

Price, G. F., Batzel, T. D., Comanescu, M., & Muller, B. A. (2008). Design and Testing of a Permanent Magnet Axial Flux Wind Power Generator. *Proceeding of the 2008 IAJC-IJME International Conference* . Nashville.

Shelton, M. L. (1994). *The Next Great Thing: The Sun, the Stirling Engine, and the Drive to Change the World.* New York, NY: W. W. Norton and Company.

Smyth, C. (2014, December 2). *3D Printing for Beginners*. Retrieved March 9, 2016, from http://3dprintingforbeginners.com/stop-3d-printing-everything-in-one-piece/

Stratasys ABSplus. (2016). Retrieved from Stratasys.com:

    http://www.stratasys.com/materials/fdm/absplus

Swisher, R. (2014, February 13). *Fast, Good or Cheap. Pick Three?* (Business.com)

    Retrieved March 29, 2016, from http://www.business.com/management/fast-

    good-cheap-pick-three/

Urieli, I., & Berchowitz, D. M. (1984). *Stirling Cycle Engine Analysis.* Bristol, England:

    Adam Hilger Ltd.